UNIVESITY OF CYPRUS

THESIS

DESIGN OF THERMOELECTRIC GENERATOR FOR WASTE HEAT RECOVERY FROM MARINE INTERNAL COMBUSTION ENGINES

Georgios Constantinou

DEPARTMENT OF MECHANICAL AND MANUFACTURING ENGINEERING

JUNE 2023

DEPARTMENT OF MECHANICAL AND MANUFACTURING ENGINEERING

Design of thermoelectric generator for waste heat recovery from marine
internal combustion engines

Georgios Costantinou

<u>Academic Supervisor</u>
Loucas Louca

This Thesis was submitted for partial fulfillment of the requirements for obtaining the
Master's degree in Mechanical and Manufacturing Engineering of the Department of
Mechanical and Manufacturing Engineering.

June 2023

Acknowledgment

Abstract

Large amounts of energy are released into the environment by modern ships. More precisely, the exhaust gases from internal combustion engines (ICE) on commercial and passenger ships discharge enormous amounts of thermal energy at high temperatures into the environment. Utilizing thermoelectric generator devices, which can transform thermal energy into electrical energy when there is a sufficient temperature difference, is a viable way to recover some of this energy. The purpose of this work is to suggest a thermoelectric generator for recovering waste heat energy from marine ICE exhaust gases. The proposed thermoelectric generator uses the outside surface of the ICE manifold as the hot side of the thermoelectric module, while the cold side is maintained at a low temperature through a heat sink and room temperature water flow. The target of this work is to design this thermoelectric generator and recognize the configuration that generates the maximum electric power. The analysis and design are performed with the use of modeling and simulation, while commercial software is employed to study the 3-dimensional coupled fluid flow and heat transfer at steady state conditions. A sensitivity analysis is carried out in order to identify the parameters with the highest contribution to the produced power. Besides to a full factorial optimization analysis, the more efficient Latin hypercube sampling is used. The analysis results demonstrates that substantial energy of the exhaust gases can be transformed into electric power. This is achieved with a device that is able to create the highest temperature difference between the two sides of the thermoelectric module with the use of an optimized water cooled heatsink.

Table of contents

Figures

APPENTIX

Chapter 1

1 INTRODUCTION

A major evolving issue that humanity is call to battle is global warming. Waste heat recovery systems (WHRS) and applications in industrial and residential area can reduce the amount of waste heat energy that are currently producing. Recent studies shows that different methodologies such as thermoelectric generators, heat exchangers, and Rankine cycle can be used. The optimization of these WHRS can provide a significant amount of energy savings in automotive, residential, and industrial areas. This work's main goal is to create a WHRS by designing and optimizing a TEG system with the purpose of studying its thermal dynamic behavior in order to maximize power and energy production using the exhaust gases of a maritime ICE.

1.1 Waste heat recovery applications

1.1.1 Waste heat recovery technologies in maritime applications

Generally, the waste heat in a marine ship is the energy of the fuel that is wasted in the environment from the ship's diesel engine and other operations. From the total fuel energy about 50% is rejected to the atmosphere [1]. Each year ships Internal Combustion Engines (ICE) discharge massive energy and carbon emissions to the environment. Carbon emissions have increased 8.4% from 2012 to 2019 according to the International Maritime Organization (IMO), [2].

WHR potentials are connected directly to the available temperature range of different ship engine's waste heat sources; the waste heat incinerator, the engine exhaust gas, the compressor outlet and the engine's cooling water. The temperature ranges for every different waste heat source of the engine is presented on Table 1. Every different WHRS can offer a solution to a different waste heat source. Recent studies shows that a variety of methods such as, Rankine cycles (RCs) the organic Rankine cycle,

supercritical Rankine cycle, Kalina cycle, exhaust gas recirculation (EGR), turbocharging, thermoelectric generators and exhaust heat exchangers can be a promising solution to recover the waste heat from engines [1,3].

Table 1:Temperature range of ship engine's different positions [1]

Engine position	Temperature range
Incinerator	850-1200°C
Exhaust	200-500°C
Compressor outlet	100-160°C
Engine's cooling water	70-125°C

Rankine cycle is a common way to produce electricity for household use, however Rankine cycle can provide a solution as a waste heat recovery system from medium temperature sources. The Rankine cycle can be adjusted for use on marine applications and can be a reliable process due to the use of water that is available. These types of systems can be easily use by marine engineers and can offer a good recovery potential in contrast with the low temperature sources [1].

Organic Rankine cycle (ORC) can be used onboard at low temperature sources. Mondejar et al. [4] review the use of ORC for waste heat recovery in marine applications and as a result the ORC using low-sulfur fuels can save between 10% to 15% of fuel by recovering waste heat from engine's exhaust gases.

Kalina cycle is a high efficiency system due to the non-isothermal phase change properties of the ammonia-water working fluid. Larsen et al. [5] studies the Kalina cycle as an efficient system for waste heat recovery in exhaust of marine diesel engines. This investigation proposes an optimized cycle with reheat and a uncommon process called split-cycle. The results of this study show that the proposed optimized Kalina cycle can obtain a thermal efficiency of 23.2% when reheat is used.

EGR system is a popular and cost-effective solution to reduce NO_x emissions and also can be used for waste heat recovery in marine engines combined with a steam cycle [3]. In EGR systems a percentage of exhaust gas is recirculated back to the engine, and the amount of exhaust gas that is recirculated depends on engine load. Also taking into

consideration the impact of shipping industry emissions to the environment the and the strict regulations, a lot more interest is given to combined power cycles. Combined cycles can minimize the emissions and maximize the efficiency and maximum power output. Kim Sørensen et al. [3] study the use of EGR combined with two different configurations of steam Rankine cycles, a 2-pressure level steam cycle compared to a 3-pressure level steam cycle. This study shows that the three-pressure level steam cycle can produce 1641 kW of power in compared to the 2- pressure level steam cycle that produce 1577 kW of power.

1.1.2 *Waste heat recovery using thermoelectric generators*

Thermoelectric generators can be used to recover waste heat energy from various industrial processes, automotive and marine engines. Despite their low conversion efficiency TEGs have many advantages. They can produce electricity by using only thermal energy and also have an extended service life compared to other devices. TEGs have no moving parts, and they are solid structures that has low volume and weight. Furthermore, they can be installed at any location or orientation.

The main advantage of thermoelectric generators (TEG) is that they can produce electrical power by converting the waste heat into useful electrical energy. X. Liu et al. [6] study the performance of a Bi2Te3 TEG system for energy harvesting to extract heat from an exhaust pipe of an automotive ICE and convert the waste heat energy into electrical power. The tests show that cold side flow rate, applied pressure, and cold side temperature can significantly affect power generation of TEG system. Lee, J. et al. [7] demonstrate that electronic doping-induced surface charges in PbTe particles can improve the viscoelasticity of Inks in order to be used in a tube shape for energy harvesting in automobile exhaust gases. The results show that the fabricated material can simplify the system, minimize the production costs and increase the performance of the TEG system. Furthermore, extended range electric vehicles (EEVs) are a suitable application for a TEG system because extended range electric vehicles run primarily on electricity and the ICE of these vehicles is used as a supplementary power unit. Song Lan et al. [8] study the use of a TEG waste heat recovery system to an EEV ICE. The results show that TEG applied on conventional vehicle have 1.7% more fuel consumption that TEG applied in EEVs.

TEGs can be used also for low-grade recovery of waste heat in large scale applications such as heat exchangers in industry. A study investigates the TEG performance with a compact thermal design of the heat exchanger in order to show that this units can demonstrate a density power of 86.4 kW/m^3. Another industrial application of thermoelectric generators is the industrial approach that was developed by KELK Ltd that experimented by using thermoelectric generation system at a carburizing furnace for waste heat recovery [9]. The hot side of TEGs is heated from the residual carburizing gas. This TEG system consists of multiple devices with 16 Bi-Te modules each. The hot side temperature varies from 50 to 250 ºC and on the other hand the cold side temperature was kept constant at 30 ºC. Results shown that 214 W of electric power was produced, which was used to charge batteries and to power LED lights.

In summary, TEGs can provide a solution also for maritime industry as the previous applications shown. In this work the installation of thermoelectric generators on marine ICEs and will be investigated.

1.2 The thermometric modules

The thermoelectric principle is a coupling between heat and electricity inside the thermoelectric material. The thermoelectric effect is the electrical potential generation across the conductor material by creating a temperature gradient between the two sides of the thermoelectric module [10].

TEG modules are working in two different ways due to the two phenomenon that occurred, the Seebeck effect for power generation and the Peltier effect for heat pumping. The Seebeck thermoelectric effect is the generation of a voltage difference by applying a temperature difference. The result of this phenomenon shows that the module operating mode is the power generation. An electrical current is produced by heat flowing through a thermoelectric module, depending on the temperature difference across it.

A TEG module consists of multiple thermoelectric pairs of p-type and n-type legs made of highly doped semiconducting materials [11,12]. The TEG module contains several thermoelectric n-type and p-type paired legs that are built of highly doped

semiconducting materials [11,12]. The electrical connection of the legs is in series in order to increase the voltage; however, the two sides of all legs have the same temperature (thermally connected in parallel). The legs are enclosed between two ceramic plates for electrical insulation (Figure 1).
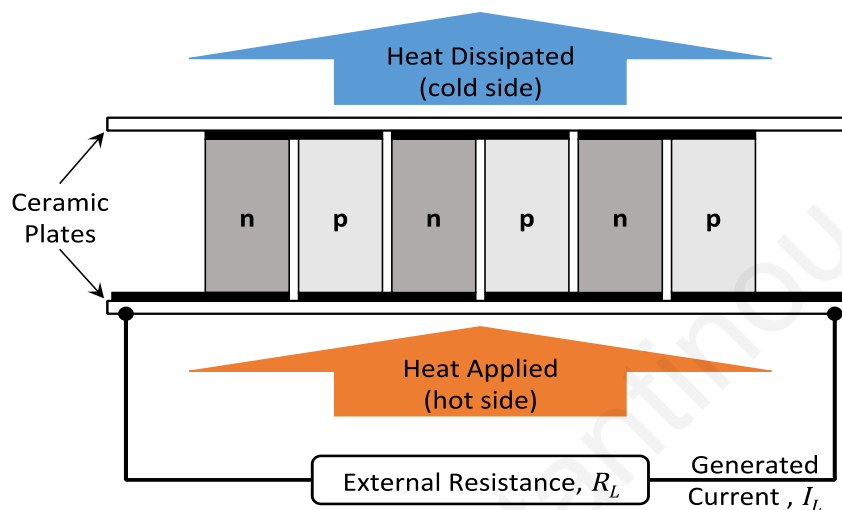
Figure 1.1: TEG module configuration

The p-type legs are positively charged due to the lack of electrons and a current flow is created when a heat flow exists. Heat and current flow have the same direction. On the contrary, n-type legs have a negative charge so current and heat are counter flowing. Due to the series connection, the voltage produced by each pair is added to create the overall module voltage. The power that a thermoelectric generator produces is capable of powering standard electrical or electronic devices.

1.3 Marine ICE system

Generally, the waste heat from the ICE comes from exhaust gases at high temperature. As a result, the available positions for the TEG device to operate is after the combustion chamber. The exhaust gases for a typical 7-cylinder ICE with engine power 7 to 12 MW are used and the temperature of the exhaust gases is around 370 ºC. This turbocharged engine series operates in typical commercial ships and its overall power depends on the number of cylinders (5 to 8), rotational speed (95-124 RPM) and engine configuration. It has a 500 mm bore, 2010 mm stroke and a length of 7.34 m for 7 pistons.
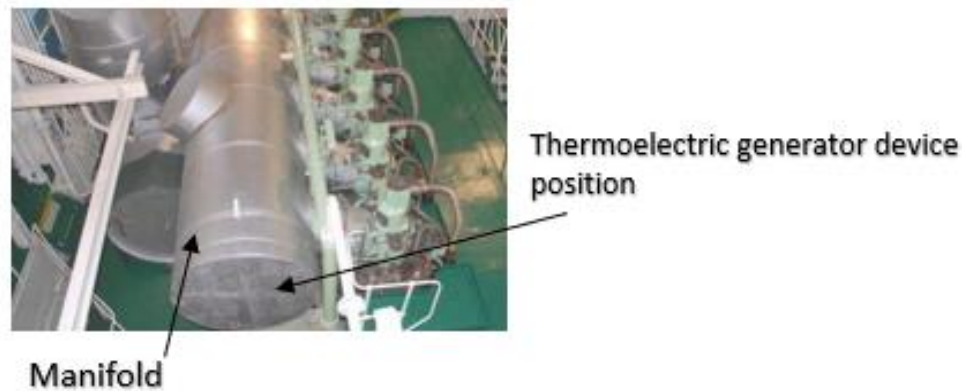
Figure 1.2: ICE manifold

There are many different available positions that a TEG device can be installed, like the cylinder exhaust port, bypass the engine system, engine manifold outside surface, and ship incinerator.

1.4 Thesis goal

The aim of this thesis is to design and optimize a TEG system that generates the maximum possible power using the waste heat energy of maritime ICEs exhaust gases. First, the methodology of Finite Element Method and the Latin Hypercube Sampling approach are described in the next sections. Then, the overall design procedure, the simulation model, and postprocessing procedure are provided in the system and geometry chapter. Next, the initial studies and final model are presented in chapter 3 and 4 respectively. Furthermore, the parametric analyses are presented in chapter 5, and finally, conclusions are given.

CHAPTER 2

2 BACKGROUND

2.1 Finite elements and solvers

The finite element method (FEM) will be used to solve the partial differential equations that describe the behavior of the model. With FEM, the complex and nonlinear differential equations can be solved for the complex geometries of the domains of interest. For this work, the commercial software COMSOL Multiphysics is used [13, 14]. For this model, the interaction between the heat transfer differential equations and the laminar flow differential equations will be used.

A sample model is presented in Figure 2.1Figure 2.2 in order to describe the computational procedure. The model below is structured as a basic heat exchanger model where an external solid steel tube with an internal flow of cold air (20 °C, 0.2 m/s) and with an internal steel tube with an internal flow of hot air (270 ºC, 0.1 m/s). This model is created to observe the behavior of non-isothermal flow conditions and the flow effects in the actual model computational studies.
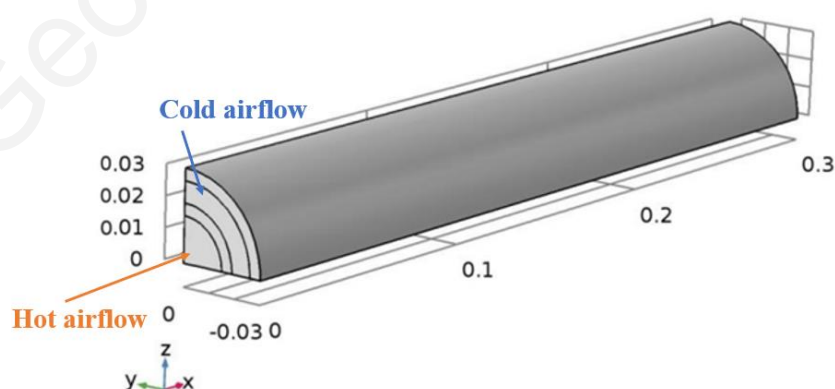
Figure 2.1 :Example model

The mesh consists of 772848 domain elements, 75090 boundary elements, and 2610 edge elements (Figure 2.2). The overall computational time was 4 minutes and

39 seconds with PARDISO solver in a computer with an Intel(R) Xeon(R) W-2125 CPU 4.00GHz, 4 cores processor and 128 GB of RAM memory.
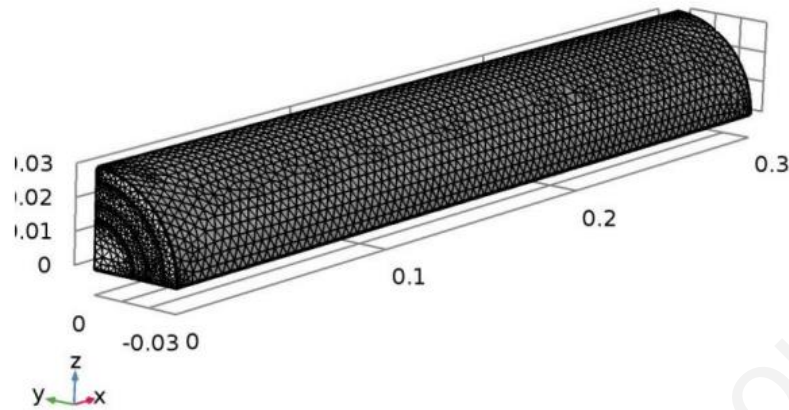
Figure 2.2: Example model mesh

The equations for the heat transfer are solved by the FEM for the entire computational volume. The general differential equations are presented in Equations (1) and (2) and their solution determines the temperature, T, and heat flux, q. The required parameters to solve the equations are the density of the fluid and solid density ρ, specific heat capacity for solid and fluid material C_p, thermal conductivity for solid and fluids k. In addition, the velocity field that is defined by the coupling with the stationary incompressible laminar flow is needed. For this work, the differential equations are used in a stationary form, where the time dependent terms are eliminated from the equation. Equation (2) describes the relationship of heat flux with the temperature gradient. In this work, this relationship is crucial due to the non-symmetrical tensor that this equation provides.

$$\rho C_p \vec{u} \cdot \nabla T + \nabla \cdot \vec{q} = Q \tag{1}$$

$$\vec{q} = -k\nabla T \tag{2}$$

The solution of Equations (1) and (2) requires the definition of the appropriate boundary conditions. For the analysis in this work, two different forms of boundary conditions are used. Taking into consideration the example above in Figure 2.1 the outside area of the external steel tube is considered as a surface with thermal insulation, the heat flux is zero, and this condition is expressed by Equation (3). Moreover, on

surfaces with interaction between the ambient air and the device for example the internal tube area, there is heat transfer by means of convection and this heat flux is expressed by Equation (4). In these equations, h is the convection coefficient, $\vec{n}$ is the unit vector normal to the outside surfaces, and T_{amb} is the ambient temperature.

$$-\vec{n} \cdot (-k\nabla T) = 0 \tag{3}$$

$$-\vec{n} \cdot (-k\nabla T) = h \cdot (T_{amb} - T) \tag{4}$$

The COMSOL software has a variety of FEM solvers that can be used for the simulation with Multiphysics phenomena and interactions. The use of each solver depends on the convergence of the model and the available processing power. Different types of solvers have been used to evaluate the computational time and convergence. The MUMPS solver was unreliable for this type of simulations due to the complexity of the multiphysics at large mesh studies. As a result, the solver that is chosen is the segregated solver with Parallel sparse Direct Solver (PARDISO) [15]. PARDISO is one of the best methods to solve large mesh problems faster because in large scale simulations with nodes that are zero, sparse matrix algorithms can reduce the computational time from the fact that in their matrices, they do not include the zero nodes in data storage. On the other hand, PARDISO solves all matrixes in parallel, this means that the solver is using huge RAM memory space for multiphysics studies and if is unavailable it can create a lot of complications regarding the computational time. In this case the computer that is used has 128 GB of RAM, 30% more that the needed RAM memory.

The results that extracted are the model temperature, velocity and pressure difference between entrance and exit of the flow. The temperature profile in [K] is presented in **Error! Reference source not found.**. The temperatures shows that the "heat exchanger" example study is in an agreement with the temperature values that are expected. A heat flow from the hot air towards the cold air is observed.
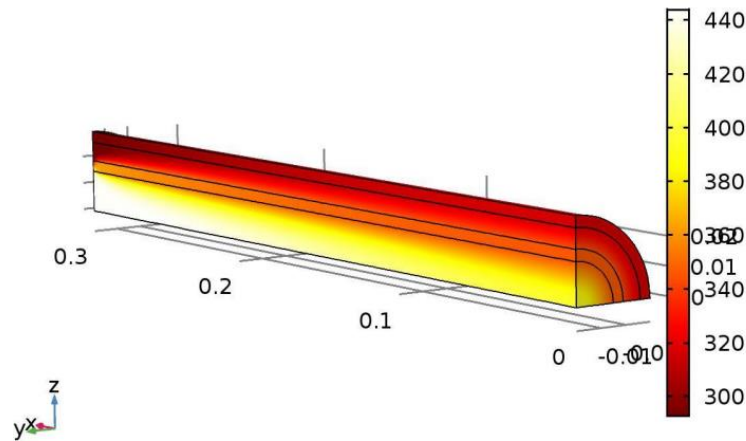
Figure 2.3:Model temperature in Kelvin

2.2 Latin hypercube

Generally Latin Hypercube Sampling (LHS) is a method that attempts to allocate random numbers evenly over a multidimensional parameter space [16,17]. The advantage of this method over an ordinary random sampling is that the LHS can distribute the parameters evenly around the center of the parameter space. This is particularly beneficial when large number of parameters need to be evaluated and/or time-consuming computations are required for evaluating the performance of each parameter set. The LHS approach enables uniform coverage of the design space while limiting the number of the parameter set points to a minimum, which in turn reduces evaluation time. An example of a two-dimensional LHS with twenty-one points is shown in Figure 2.4, where each '*' represents a point of the parameter set. Note the uniform coverage of the two-dimensional space with at least one point for each value of X_1 and X_2 (column and row). Covering the same space with a full factorial approach would require $21^2 = 441$ points. Moreover, an advantage of LHS is the flexibility that it provides. In this case, if one of the set of parameters must be eliminated from the study due to geometric limitations, the existing data can still be used without a reduction in the evaluation points. In this study, the use of LHS can help determine the area of interest and allow the examination of a larger range of values.

Figure 2.4: LHS−2D space sample.

CHAPTER 3

3 SYSTEM MODEL AND GEOMETRY

3.1 Thermoelectric device system

The thermoelectric device system consists of different components that work together in order to produce power from the exhaust gases waste heat. For this study the outside area of the manifold is chosen (Figure 3.1) and more specifically the two circular flat surfaces at its ends (380 mm in diameter). This location was selected after discussions with the marine engineers who pointed out that minimum modifications during the installation of the TEG is critical. Nevertheless, the proposed method can be used to investigate other installation locations. Nevertheless, the manifold position is chosen since is the least intrusive to the ICE system, which leads to simpler modifications for the installation and it has the larger outside temperature compared to other positions external temperature. Bearing in mind the exhaust gases temperature and the temperature losses, a conservative approach is used and the temperature on the exterior surface of the manifold is set to be 270 ºC, where the hot side of the TEG will be installed.

Figure 3.1: Thermoelectric device position

The proposed thermoelectric device contains the following three main parts: the heat expansion plate (1), thermoelectric modules (2), and the water cooled heatsink (3),
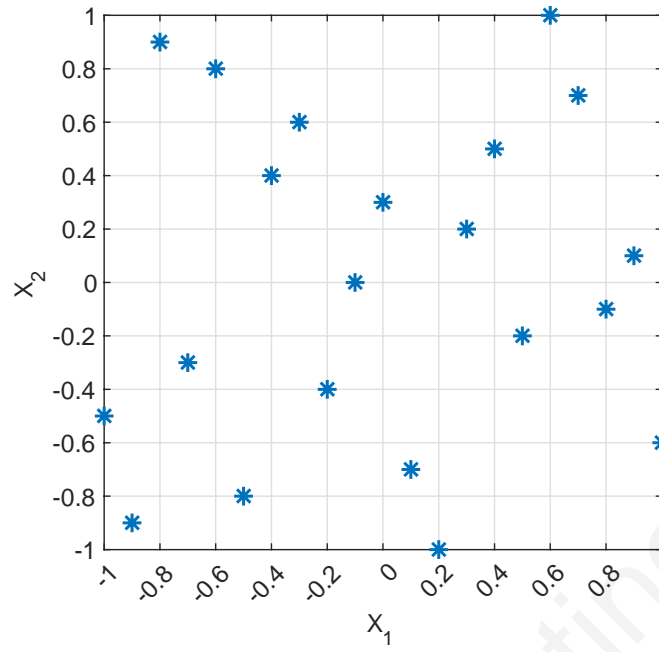
as shown in Figure 3.2. The area between the TEG modules is assumed to be static air. To achieve a high temperature difference between the hot and the cold side of the modules, the modules are sandwiched between the cooling heatsink and the heat expansion plate. The heat expansion plate is responsible for the isothermal temperature allocation in all the TEG modules and is in direct contact with the outside surface of the manifold. The device has a square profile with overall dimensions 360×360 mm in order to fit with the circular end of the manifold end. It includes a total of 36 modules that are 50×50 mm each and they are arranged in a 6×6 pattern. These dimensions allow for an 8 mm gap between the modules and a 10 mm empty space at each end. These gaps are necessary for electrical connections and cables that run from each module to the outside connections of the TEG.
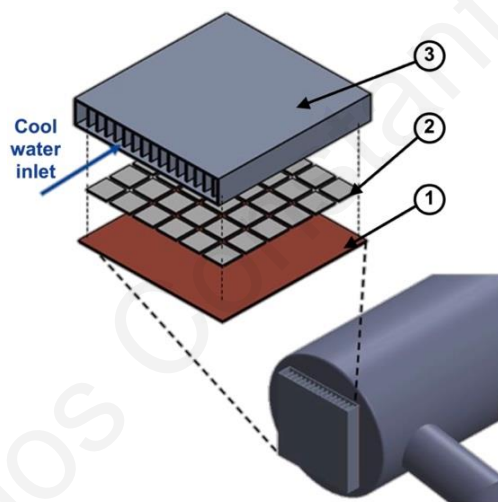

Figure 3.2: Exploded view of TEG device.

The cooling heatsink is an enclosed rectangular tube that allows the flow of the water from the one side to the other in order to extract heat and create a low temperature on the cold side of the modules. The lower surface of the heatsink is in contact with the modules. The inside area of the heatsink includes longitudinal fins that increase the overall heat transfer area and therefore the heat transferred from the modules to the water. The cross section of the heatsink is shown Figure 3.3. The fins can have a variable height and width that will be determined later using the parametric studies. In addition, the number of fins or gap between the fins is variable. Initially the heatsink has an overall height of 60 mm and 15 fins.
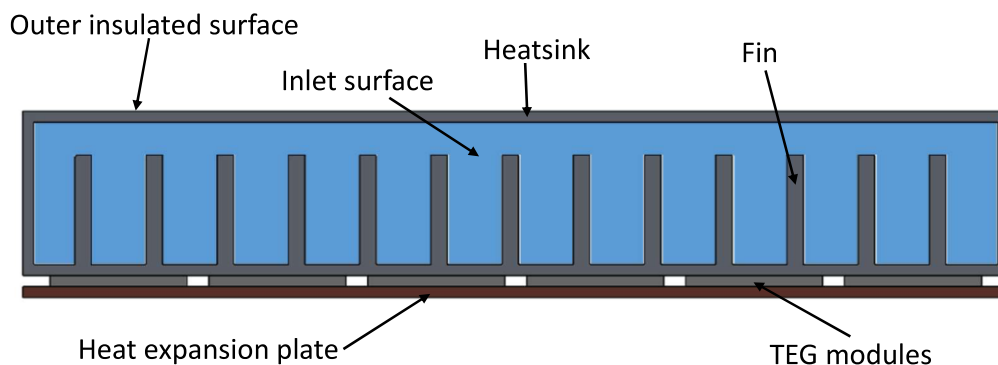
Figure 3.3: Front view of TEG device

3.2 Parametric geometry

In order to create a geometry that changes for different parameter sets the model geometry has to be parametric. The parametric geometry is an essential segment of the methodology process in order to create a model that provides efficiency and accuracy in terms of procedure. Model geometry for a given the values of a parameter set is calculated through the formulas given in Table 2. The parameters set is affecting every geometric characteristic that determine the shape of the model. The model that is presented in Figure 3.4 is constructed with overall height of 60 mm and 29 fins with 4 mm width.
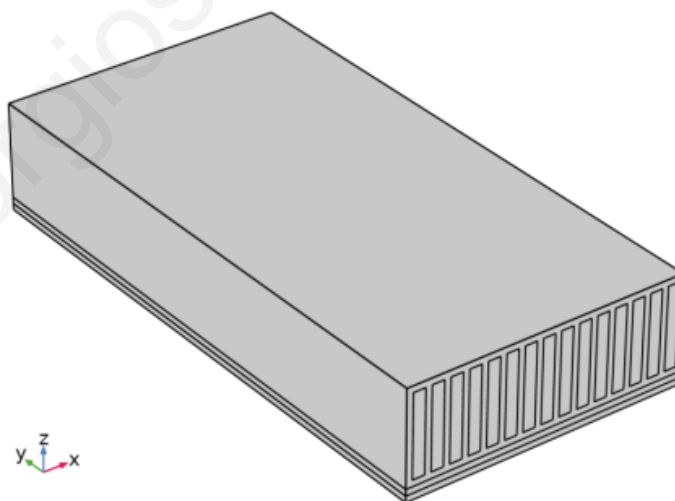

Figure 3.4: Typical model geometry

The geometry of the model is designed inside COMSOL using a set of parameters that describe each characteristic of the model geometry. The exact model geometry is defined by three parameters of the fins: number, thickness, and height. These parameters will be later varied by the parametric studies to identify the most sensitive

parameters to maximize the produced net electric power. Furthermore, note that by varying these parameters the inlet velocity is changed due to the change of inlet surface. Using the heatsink height and subtracting 8 mm (2 times the 4 mm wall thickness) the overall fin height is calculated. The channel thickness is calculated using the number and the thickness of the fins. In addition, from the thickness and height of the fins the entrance area of every channel can be calculated and also the overall entrance area.

Table 2: Parametric design parameters

Parameter	Calculation formula	Description
h_heatsink	60 [mm]	*Heatsink height*
t_fin	4 [mm]	*Fin thickness*
n_size	30	*Number of fins*
h_fin	h_heatsink-8 [mm]	*Fin height*
t_chan	(352-n_size*t_fin)/(n_size+1) [mm]	*Channel thickness*
Entry_area	(t_vent*(n_size+1)*h_fin) [mm^2]	*Inlet area*
Q_entry	0.0004 [m^3/s]	*Volumetric flow*
v_entry	Q_entry / Entry_area [m/s]	*Water velocity*

To take into consideration the velocity changes for different geometries during the parametric study the velocity for each parameter set is calculated considering a constant volumetric flow. This type of geometric model setup allows the easy implementation of parametric studies without constant supervision of COMSOL or having to run each simulation separately.

3.3 Model boundary conditions

The TEG device model, with its three-dimensional geometry, includes non-isothermal flow with laminal incompressible flow conditions and conjugate heat transfer at the interface between the fluid and the heatsink. The multiphysics model behavior and interactions are described by the partial differential equations in Section 2.1.

A vital part of the model are the boundary conditions as shown in Figure 3.5. For the heat transfer, the inlet temperature is set to a constant 20 ºC and for the outlet is set to "outflow" that enforces heat transfer only by convection. The outside surface of the

device is assumed adiabatic due to the insulation of the manifold enclosure for safety reasons. The outer surface of the heat expansion plate is set to be 270 ºC, which is the temperature of the manifold. For the flow, the inlet surface boundary condition is set to constant velocity, where the outlet surface is set to constant pressure (atmospheric). The inlet water velocity is determined by the volumetric flow that is kept constant 0.4 liters/s. For the parametric studies the velocity is changing due to the different inlet surface for each set of fin parameters. This assumption ensures that the cooling capacity is constant and therefore only the effect of the heatsink parameters will be accounted for the different designs. All the above boundary conditions are set to COMSOL at different physics modules that are implemented with specific equations as it mentioned in previous chapters.
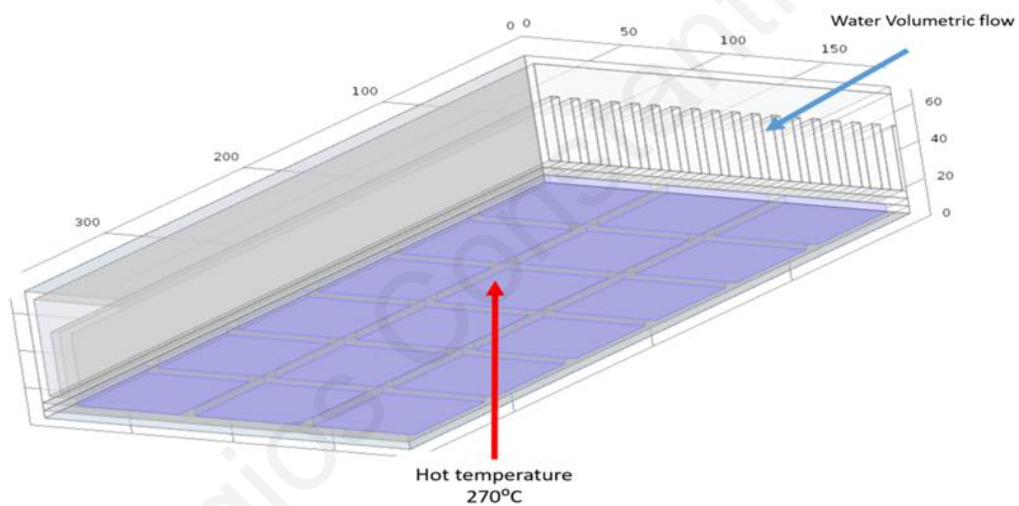

Figure 3.5: Model Boundary conditions

3.3.1 Material properties

The material physical properties are also required to perform the simulation. The material properties for the heatsink (aluminum) and heat expansion plate (cooper) are given in Table 3. These properties are assumed constant and temperature independent, which is a suitable assumption for solids. On the other hand, fluid physical properties are not constant and can be temperature dependent for both the air and the water. For water, the temperature dependency for thermal conductivity, heat capacity, dynamic viscosity, and density is used and shown in Figure 3.6. The air in the gap between the modules is considered static (solid) since it is not moving. Therefore, only thermal

conductivity and specific heat transfer are needed, and their temperature dependency is shown in Figure 3.7.

Table 3: Solid Materials properties

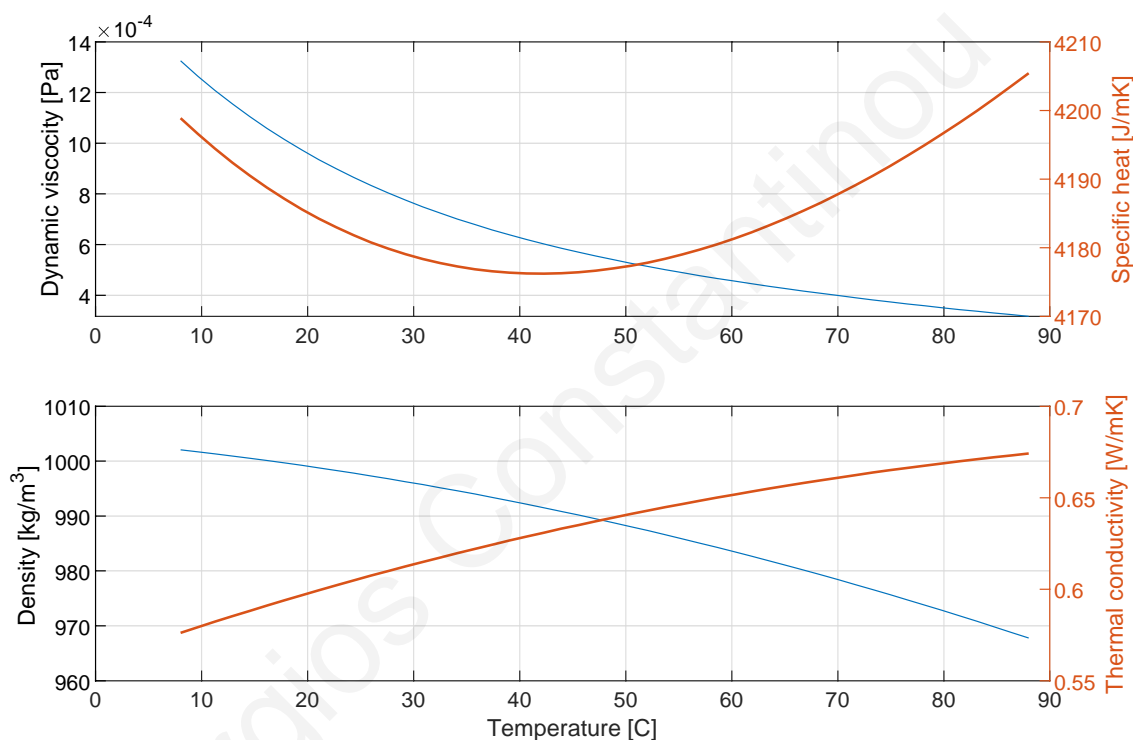| Material properties	Aluminium	Copper
Thermal conductivity k [W/mK]	238	400
Density ρ [kg/m^3]	2700	8960
Specific heat C_p [J/kgK]	900	385

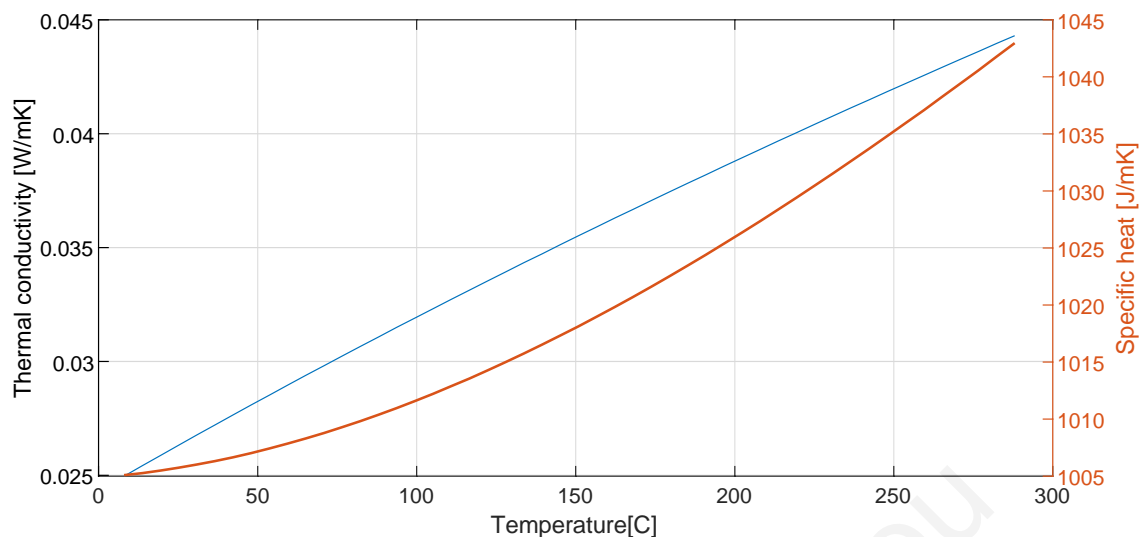
Figure 3.6: Water thermal properties

Figure 3.7: Air thermal properties

3.3.2 Thermoelectric module properties

Modules of bismuth telluride (Bi2Te3) are considered in this work. The physical properties used in the simulations and power calculations are given in Table 4. The parameters in this table are only the ones necessary for the thermal analysis of the TEG device, and they are assumed constant. In general, these parameters are dependent on temperature, but their change is insignificant for the temperature range used in this work. The dimensions of the module are 50×50×4 mm and produces maximum power when applying the temperatures provided by the manufacturer (30 °C for cold and 300 °C the hot side). The power curves for this TEG module for various cold and hot temperatures are given in Figure 3.8. These power data are provided by the manufacturer [18] and contain the thermoelectric material properties, such as the ZT and Seebeck coefficient. The specific module is selected since it is widely available on the market and can be purchased at a low price for large module numbers. Also this TEG module is selected due to its compatibility to the temperature difference of the specific implementation.

Table 4: TEG module properties.

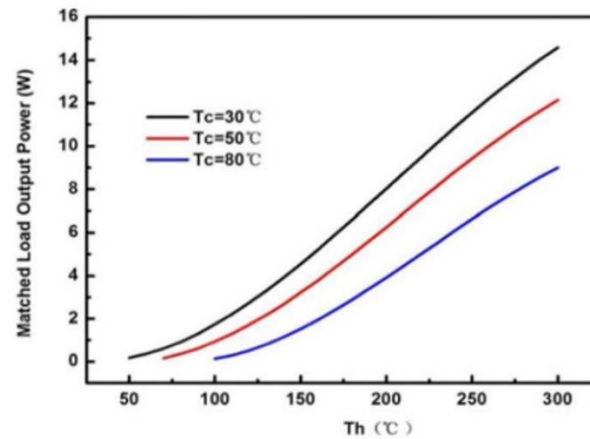| Parameters	Value
Thermal conductivity k [W/mK]	1.2
Density ρ [kg/m^3]	7700
Specific heat C_p [J/kgK]	154

Figure 3.8 :Power data of TEG module.

3.4 Initial simulation

The initial simulation is an important starting point where realistic parameters are required. A reasonable starting point is device with 29 fins with 4 mm thickness and 60mm heatsink height. The boundary conditions are set as it is shown at Section 3.3.

Mesh quality plays a significant role to simulation results; therefore, a mesh convergence is necessary in order to determine the proper mesh for the parametric studies. The pressure difference across the vents can be calculated through analytical solution [19]; so the pressure difference can be the mesh convergence parameter for this study. The analytical solution shows that the pressure difference across the channel is 2.32 Pa. Two different mesh configurations are compared with the analytical solution at Table 3 and the result shows that extra fine mesh configuration is the one that is suitable for this study. Figure 3.9 and Figure 3.10 present the pressure difference for the 2 different studies. The figures demonstrates that the distribution across the heatsink varies at a constant error. This leads to the conclusion that this error is affected only by the mesh quality.

Table 3:Mesh quality comparison.

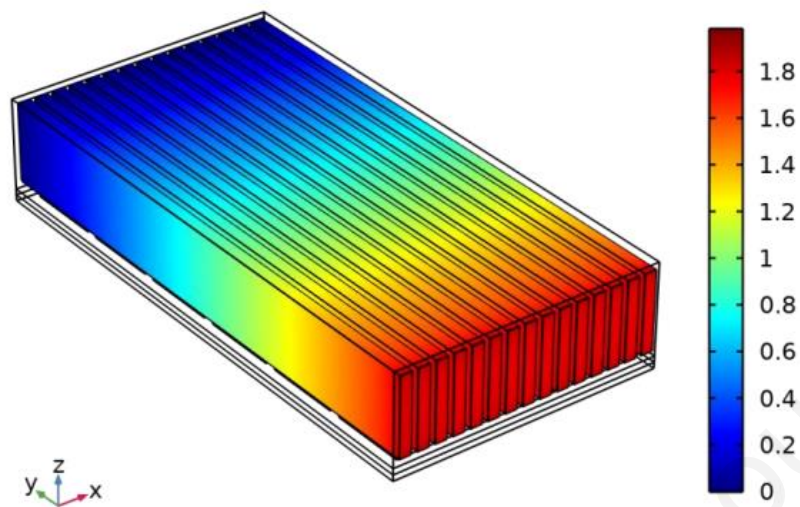| Predefined size	Fine	Extra fine
Maximum element size	5.86	2.54
Minimum element size	1.11	0.166
Pressure difference	1.6 Pa	2.12 Pa
Error	31.03%	8.62%
Computation time	3 min 10 s	31 min 40 s

Figure 3.9: Pressure difference at extra fine mesh
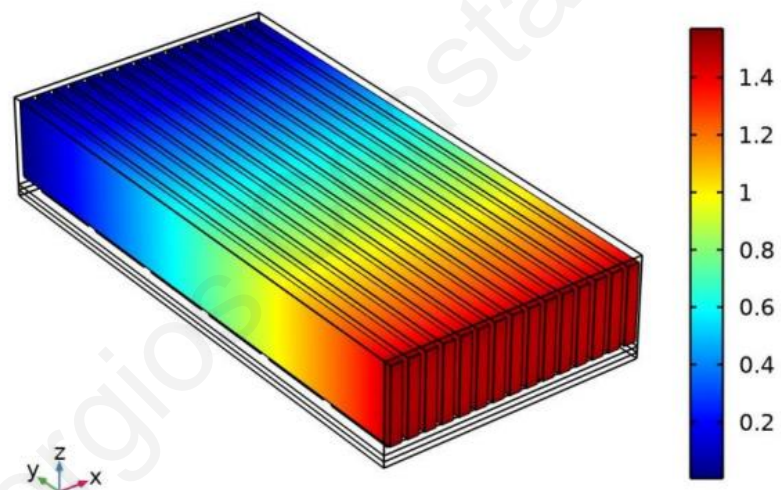
Figure 3.10: Pressure difference at fine mesh

The computational efficiency is also considered given that the FEM has about 4 million elements and requires significant amount of time to compute. This model has a simulation time of about 1 hour due to the high mesh accuracy that is required. Therefore, the model geometry symmetry is exploited to reduce the computation time. The geometry has symmetry around a vertical plane in the middle of the heatsink and this defined in COMSOL. By using this symmetry as a boundary condition, the model mesh is halved. This approach results in a model with about half the size of the original, which can be computed in about 32 minutes. All the models that are presented to this thesis are symmetric around a vertical plate in the middle of the device.

3.5 Post processing methodology

To identify the final set of parameters a MATLAB script is used. The main goal is to calculate the overall power that is produced by the modules. The temperatures of cold side and hot side are exported in high resolution from COMSOL to be analyzed. The temperature points are imported to the script and are linearly interpolated in order to get the temperature at specific points that are the same for the cold and hot side. From the new interpolated points, the power of small cells of the module is calculated. All the points are added in order to find the overall power.

First, the results for temperature, pressure and velocity are extracted from COMSOL as a result of the computational analysis.Figure 3.11: Model temperature in Kelvin For example, Figure 3.11 presents the entire model temperature.
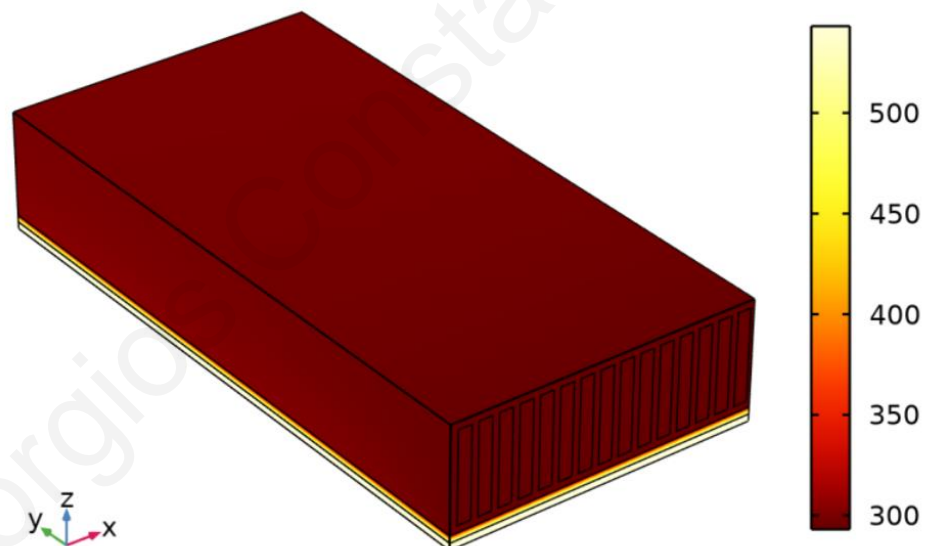
Figure 3.11: Model temperature in Kelvin

For the calculation of the net power, the surface temperatures of the cold and hot sides of the modules are also exported from COMSOL. A typical temperature profile of the cold side within COMSOL is shown in Figure 3.12. The cooling water is entering the heatsink at the left side (x=0). As it can be seen in the right plot with the mesh, the available temperatures are at the nodes of the mesh that do not necessary align with respective temperatures of the module at the hot side.

Figure 3.12: Original cold temperature surface within COMSOL

In order to get the corresponding data and calculate the net power the following procedure is used. Initially, cold and hot plate data of the thermoelectric modules are extracted from COMSOL and imported to MATLAB using the script presented in Appendix II. Moreover, the geometric inpu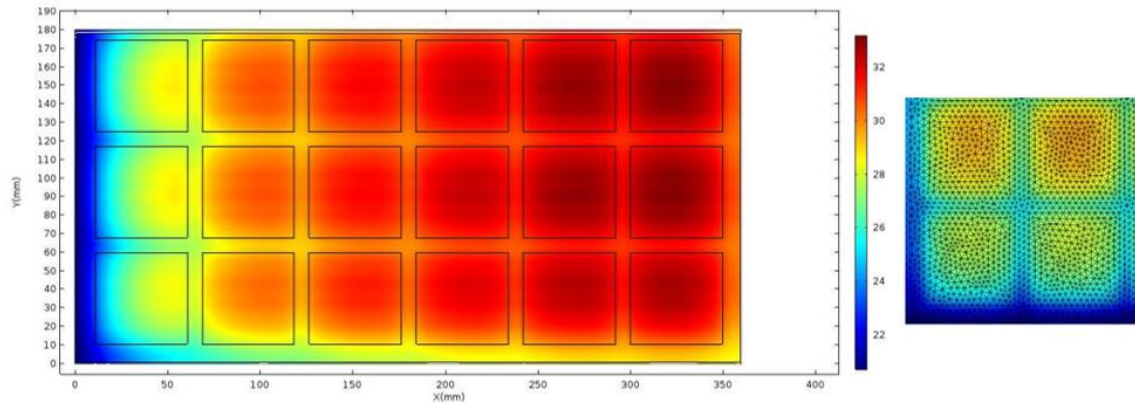ts that is necessary for power loss calculations, the module geometry pattern positions and the module data are also defined. Also, TEGs extrapolation data are calculated in order to expand the available module data space.

The next step is the linear interpolation process using built-in MATLAB functions, and the new temperature points for the cold side are presented in Figure 3.13. Then, using the equations below the calculation of power for each cell. The equation 5 is used in order to calculate the average temperature inside each cell using the four new points from linear interpolation, the equation 6 is used to calculate the area for each cell and the equation 7 is used in order to calculate the power of each cell.
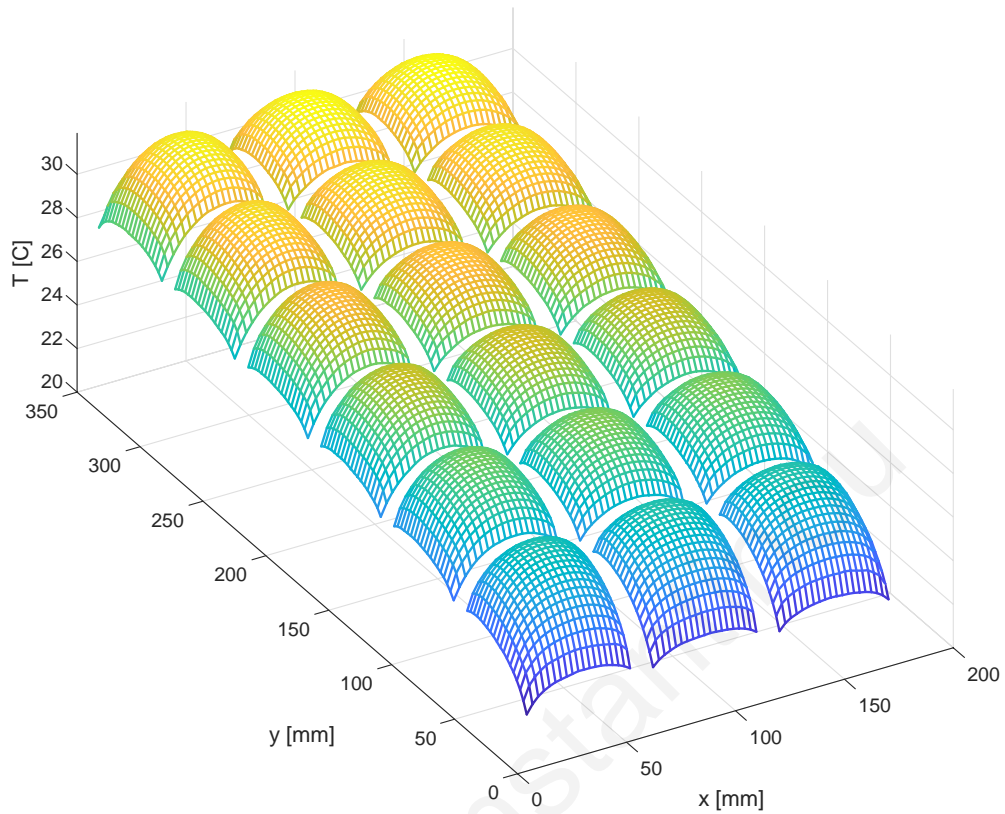
Figure 3.13:Cold side temperature at interpolation points

$$cell_{Th} = \frac{Th(i,j) + Th(i,j+1) + Th(i+1,j) + Th(i+1,j)}{4} \tag{5}$$

$$cell_{area} = \left(x(j+1) - x(j)\right) \cdot \left(y(i+1) - y(i)\right) \tag{6}$$

$$cell_{pow(i,j)} = cell_{pow_{F(cell_{Tl},cell_{Th})}} \cdot \frac{cell_{area}}{module_{area}} \tag{7}$$

In order to find the net power, the pressure losses need to be calculated. The power losses are calculated using the equations 8, 9 and 10 where DP is the pressure difference, L is the over length, c and b are geometric factors, f is the pressure losses factor and h_{maior} are the pressure losses.

$$DP = \frac{L*visc*v_{entry}}{(c^2)*\left(\left(\frac{1}{3}\right) - \frac{64*c}{(3.14^5)*b}*\tanh\left(\frac{3.14*b}{2*c}\right)\right)} \tag{8}$$

$$f = \frac{64}{Re} \tag{9}$$

$$h_{maior} = f * \frac{L*v_{entry}^2}{Dh*2} \tag{10}$$

$$DP_{friction} = dens * h_{maior} \tag{11}$$

The power that is required for the creation of the flow is subtracted from the overall power. The produced power is the sum of the individual power of all these cells. In addition, Figure 3.14 presents the power of each cell. The overall produced power is the sum of the individual power of all these cells. For example, for the specific configuration the TEG produces 367 W of net power or 2.83 KW/m^2.
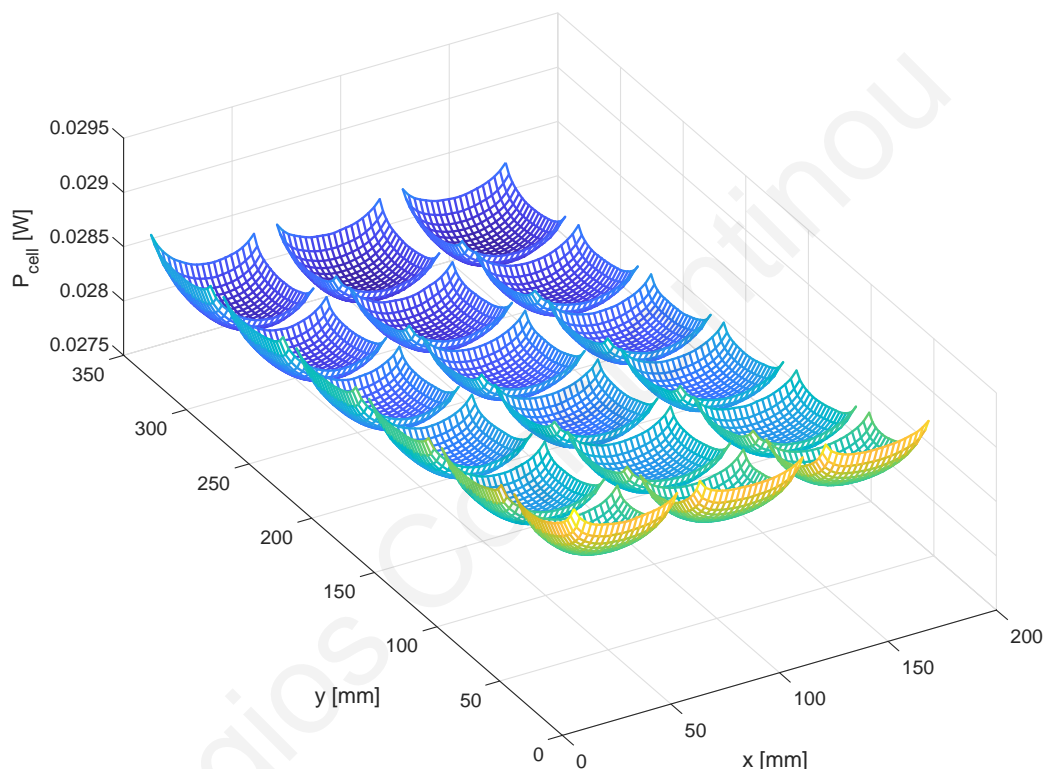
Figure 3.14: Power produced by each module cell.

3.6 Thermal resistance model

To create a reliable and accurate model, several difficulties have to be eliminated. The models that are been created in the process has shown a different problem that needs to be considered before the final studies will be performed. To identify and understand the basic principles that are occurred in the case study an 1D thermal resistance model has been developed. The 1D model provides a solution to an important factor, the validation of FEM models with analytical models when is possible. This 1D study is performed along the heatsink height in order to validate the FEM model results. The resistance model is divided into 4 different sectors. The manifold temperature, the heat expansion plate, the TEG modules and the heatsink area. The boundary conditions

of the model are considered adiabatic. The manifold and heatsink outer temperatures are considered constant due to the manifold's huge volume and the insulation at the end of the heatsink.

In order to create the 1D model a MATLAB script is created as it appeared on Appendix I. The first step is to transform the COMSOL data to different arrays since it is more convenient. Then all geometric constants are presented as it shown in

Table 4. The thermal conductivities of solid materials and the needed water parameters are imported to the script.

Table 4: 1D model geometric constants

Geometric constant	Value
Cooper plate thickness (d_cooper)	4 mm
TEG thickness (d_teg)	4 mm
Aluminum heatsink solid part	4 mm
Fin area height (d_conv)	52 mm
Fin length (l_fin)	40 mm
Fin thickness (t_fin)	4 mm
TEG module area (a_teg)	50mm x 50mm

Furthermore, all the calculations are performed using the equations below. The required parameters to solve the equations are the density of the water (*dens*), the specific heat of water (C_{pwater}), the viscosity of the ($visc_{water}$), the thermal conductivity of water (k_{water}) and the velocity (*v*) of water in order to calculate the Prandtl number (*Pr*) and Reynolds number (*Re*) using equations (5) and (6) respectively. In addition, the Nusselt number is calculated from the equation (7). The characteristic length (L_C) and dimensionless parameter (*m*) is calculated through the equations (8) and (9) respectively. Moreover the overall fin efficiency (n_f) using the equation (10) and the A_{fin} area using the equation (11).

$$Pr = \frac{cp_{water} \cdot visc_{water}}{k_{water}} \tag{5}$$

$$Re = \frac{dens \cdot v \cdot d_{conv}}{visc_{water}} \tag{6}$$

$$Nu = 3.61 + \left(\frac{\left(0.065 \cdot \left(\frac{d_{conv}}{1} \right) \cdot R_e \cdot P_r \right)}{1 + 0.016 \cdot \left(\frac{d_{conv}}{1} \cdot Re \cdot Pr \right)^{\frac{2}{3}}} \right) \tag{7}$$

$$L_c = L + \frac{t}{2} \tag{8}$$

$$m = \sqrt{\frac{2 \cdot h \cdot t}{k_{water}}} \tag{9}$$

$$\eta_f = \frac{\tanh m\, L_c}{m\, L_c} \tag{10}$$

$$A_{fin} = 2 \cdot L \cdot Lc \tag{11}$$

The final step is the calculation of all thermal resistances in order to be able to calculate the temperatures are specific locations. Solid parts thermal resistances are calculated from equation (12) and the heatsink fin area thermal resistance is calculated form equation (13).

$$R = \frac{t}{K \cdot A} \tag{12}$$

$$R_{fined} = \frac{1}{h \cdot A_{fin} \cdot ef} \tag{13}$$

3.6.1 Model results

As a result, this validation study shows that 1D model predicts a temperature profile that can verify the COMSOL model results, as it is depicted in Figure 3.15. Some simplifications were necessary in 1D model and are barely visible in the graph. The temperature profile that is calculated in COMSOL has a small difference from the temperature profile that is calculated in MATLAB because the water velocity is considered constant in the 1D model. The difference between the TEG and the heatsink start is due to the assumption that the fin area has constant water velocity (heat flux) around the fin.
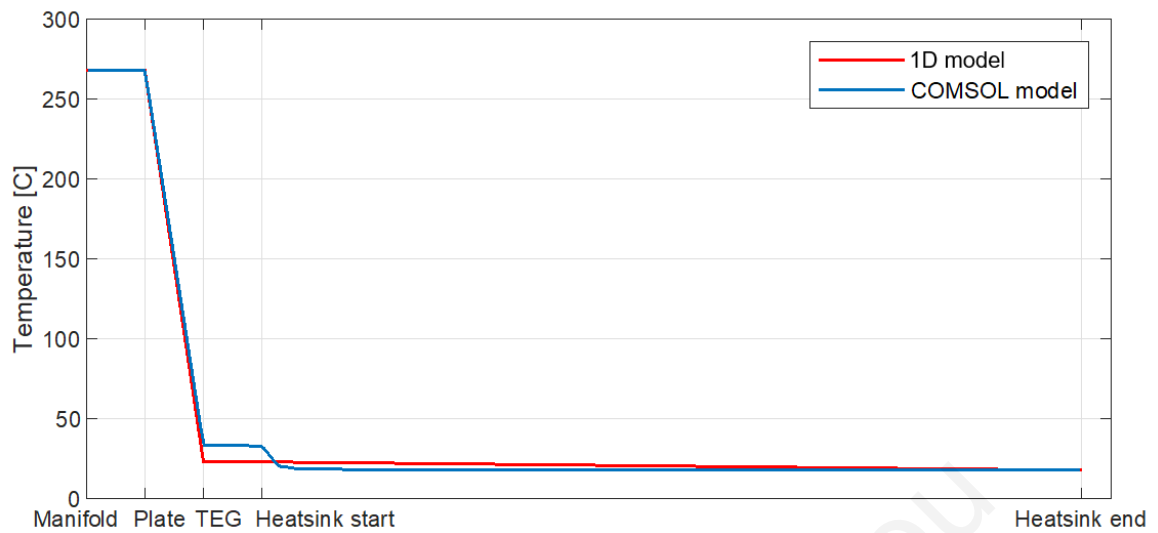
Figure 3.15: 1D thermal resistance model vs. COMSOL model.

CHAPTER 4

4 INITIAL PARAMETRIC MODELS

Some general initial studies are performed in order to identify the model that will be later used for the full factorial parametric and Latin hypercube studies. First, the fixed entrance model is investigated and then the constant volumetric flow model.

4.1 Fixed entrance model

Firstly, a fixed entrance model with a finless inlet and outlet volume is created in order to acquire a specific model accuracy. All the characteristic sizes are calculated automatically within the software as it mentioned in parametric geometry sector. The geometry is presented in Figure 4.1. The main advantage of this model is that the geometry can be used with a constant inlet speed for all parametric studies. However, the finless area at the beginning and ending of the model shows that the mesh elements are rapidly increased due to the complexity of the geometry. As a result, the higher mesh needs higher computational time without a significant impact to model's accuracy and also there isn't any substantial changes in the calculated temperature profiles. The overall model has over 5.5 million elements and needs about 1 hour to be solved.
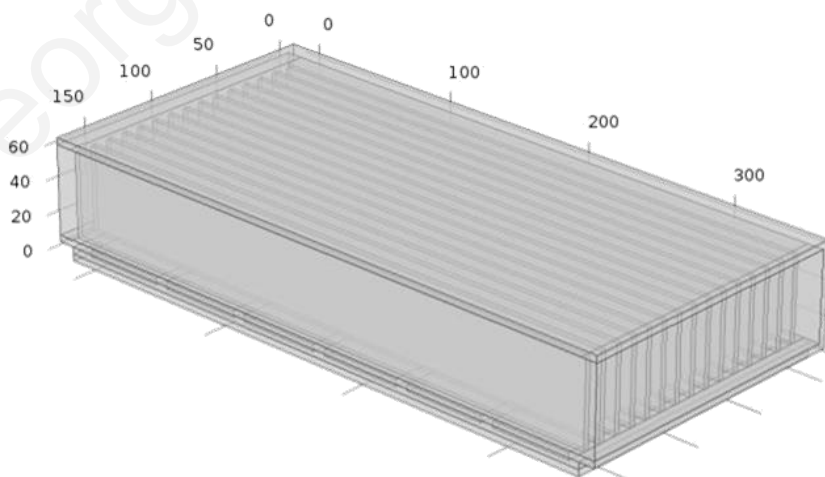
Figure 4.1: Fixed entrance geometry

4.2 Fixed volumetric flow

The inlet and outlet volumes are eliminated in order to improve the computational time through lower element number. Instead, the inlet boundary conditions are replaced with a constant velocity condition that is calculated from the given volumetric flow and overall channel area.

The results that is presented at Figure 4.2 shows that a high speed area is presented at the top of the heatsink due to the available space at the top. Having fins that do not cover the whole height of the heatsink, having a gap at the top, does not create lower temperatures at the cold side of the module, and in addition it increases the computational cost due to more complex flow. In addition, the top of the fins increases the computational time compared to the full fin model that is described to the next section.
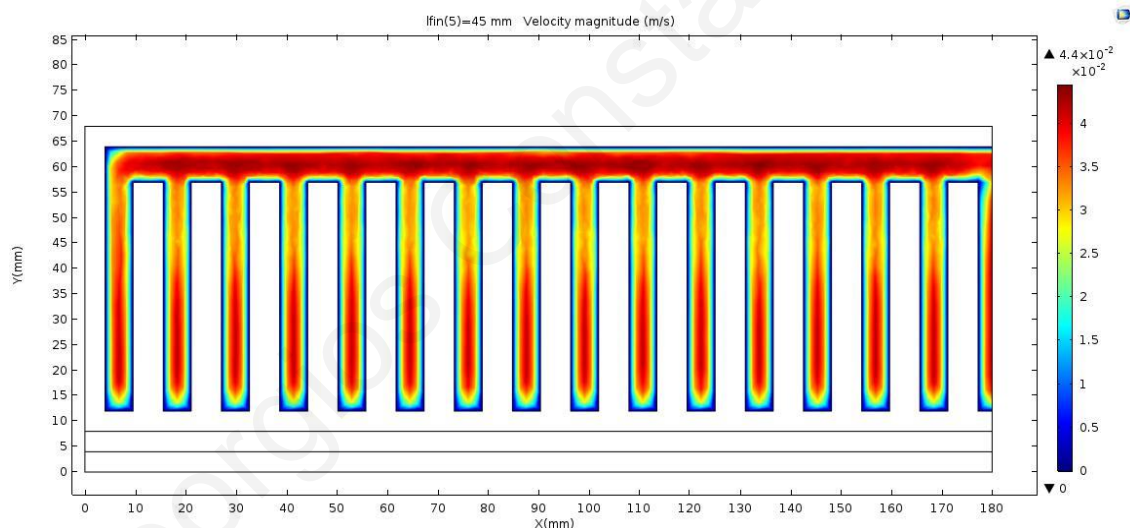
Figure 4.2: Water velocity

As a result, a new study is performed that uses full fins. considered the variation of the heatsink height with full fins. The simulation results show that the fins should cover the entire height of the heatsink in order to increase the cooling power. As a result, small rectangular channels form across the width of the TEG device and the final geometry is shown in Figure 4.3**Error! Reference source not found.**.
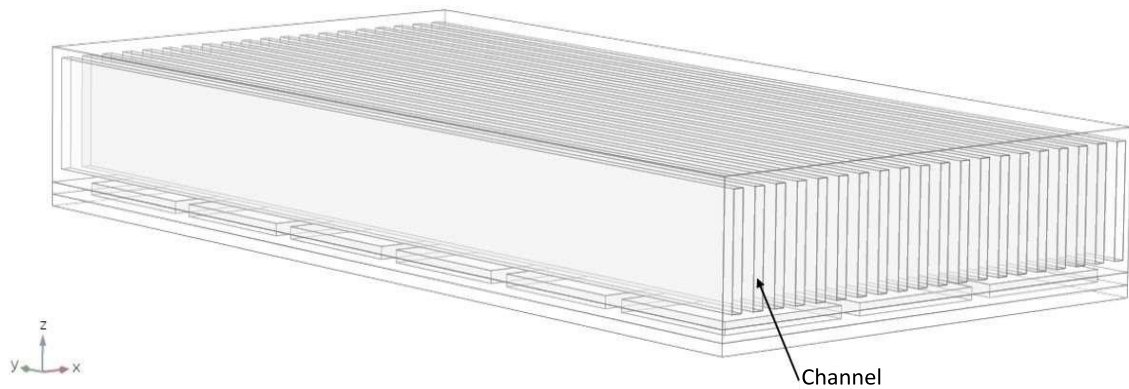
Figure 4.3: Final model geometry

4.3 Parameter combination studies

Also, the effect of each heatsink parameter to the temperatures, for full height fins, is studied. This analysis showed that the three most significant parameters are the height of the heatsink, the thickness and number of the fins inside the heatsink. The combination parameter studies are needed in order to determine the range of each parameter that is required to the two final study modes, the full factorial and Latin hypercube studies. The studies of each individual parameter show that there is no need to study a lower number of fins than 33, the fins thickness range is 3-7 mm and the heatsink height range is 30-60 mm. An example of parameter study for different number of fins is shown in Figure 4.4: Example of cold plate temperature for different number of finsFigure 4.4. This figure shows the temperature at the middle of TEGs cold surface from the start to the end of the heatsink, in the direction of the water flow. The example results demonstrates that the selection of each parameter space is vital in order to create a desirable temperature difference that provides the maximum net power that can be produced by the system. Also note the variation of the temperature in the x-direction due non-uniform material under the heatsink. The area under the heatsink consists of a thermoelectric module and air caps all around it, resulting in non-constant thermal resistance and thus temperature variations in the x-direction.
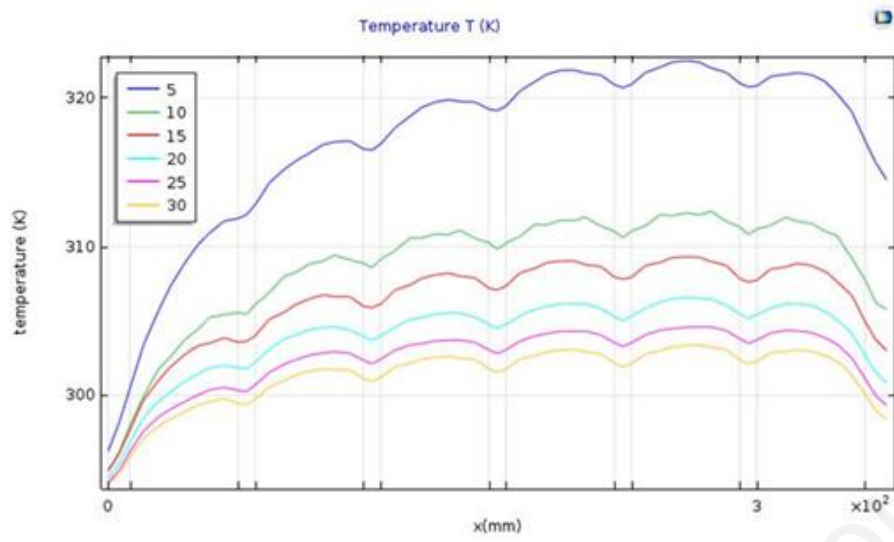
Figure 4.4: Example of cold plate temperature for different number of fins.

CHAPTER 5

5 PARAMETRIC STUDIES

The parametric studies are performed in order to evaluate the effect of a variety of possible combinations of the device parameters. Based on the study performed in the previous section, it was determined that only the geometric parameters of the heatsink effect the power production significantly. More specifically, the number and thickness of fins and the heatsink height will be considered. A variety of methodologies are available for performing parametric studies and the purposes of this work two are employed, i.e., Full factorial and Latin Hypercube Sampling.

5.1 Full factorial study

A common way to explore a parametric space is a full factorial study. The parametric analysis using the full factorial approach can be lengthy since it is exponentially increasing with the number of parameters and the number of points per parameter. A high number of evaluations are required to identify the finest set of parameters. In this case we have only 3 parameters, so this approach is workable if a small number of points per parameter in used. Larger number of points can increase rapidly the number of analyses so three points per parameter are selected that gives a total $3^3 = 27$ analyses. The parameter values are shown in Table 5. These specific values are selected in order to avoid the possibility of having a negative channel thickness, which creates a non-real model that cannot be simulated. The number of fins has to be odd in order to avoid a half fin at the middle and increase the model complexity.

Table 5: Full factorial parameter values

Parameter	Value
Fin thickness	3, 5, 7 [mm]
Heatsink height	30, 45, 60 [mm]
Number of fins	25, 35, 45 [-]

The main goal of full factorial parametric study is to identify the parameters with the highest contribution to energy recovery. This is achieved with the calculation of the several set of parameters. The produced power without and with the power loss needed

to create the necessary water flow are calculate the results are shown in Figure 5.1. The results confirm the effect of power losses for creating the required water flow. The maximum gross power produced appears at point 25 with parameter values (7, 30 45), however, after removing the flow losses the maximum net power appears at point 26 with parameter values (7, 45, 45). The higher water velocity (smaller channel area) at point 25 creates significant power losses that overcome the higher produced power as compared to point 26. Generally, the last three points have the highest power losses because of the highest number of fins and smallest channel area that create high velocity through the channels. In addition, this shows that the temperature difference cannot be an appropriate optimization parameter by itself due to the importance of power losses. The maximum net power is 367.8 W (2.837 KW/m^2) and the respective geometric parameters are 7 mm fin thickness, 45 mm heatsink height, and 45 fins.
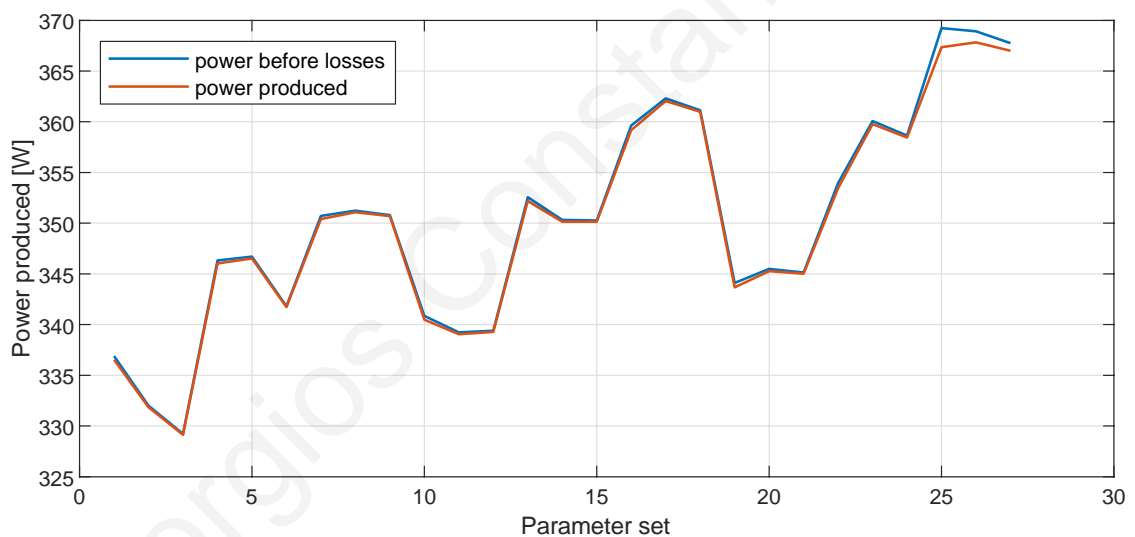

Figure 5.1: Full factorial parametric study results - power with and without losses

The pressure difference that is created at point 25 is shown at

Figure 5.3 where a high pressure difference of 1.22 KPa is created through the channel. The pressure difference of point 26 is shown in Figure 5.3. Pressure difference at point 26 is half compared to point 25.
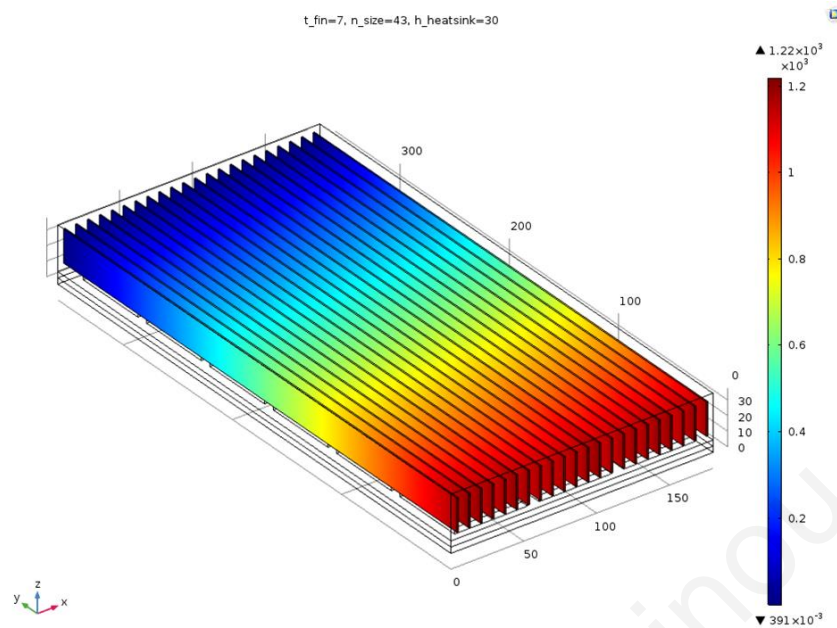
Figure 5.2: Pressure difference at point 25
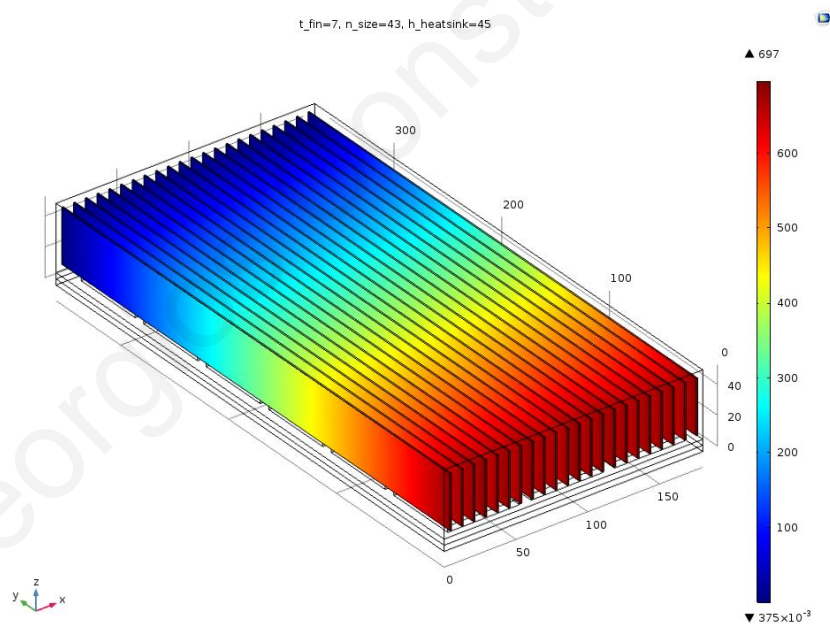
Figure 5.3: Pressure difference at parameter set point 26.

In contrast the highest cold plate temperature at 26 is only 0.2 higher that point 25 the Figure 5.5 and Figure 5.6 are presenting this outcome. Moreover, taking into consideration that the power produced by point 25 and 26 are very close, the power losses are the factor that will determine where is the maximum net power. As a result, the differences at temperature and pressure between two different set of parameters are vital factors to find the parameter set that produce the maximum net power.

Figure 5.4: Temperature at cold plate for point 25

Figure 5.5: Temperature at cold plate for point 26

5.2 **Latin hypercube**

As mentioned before, the LHS method can better cover the same parameter space with the same number of evaluation points. On the other hand, the LHS can provide a wider space of parameter sets because is independent from the number of points. The LHS parameter sets are generated using the MATLAB toolbox and they also are checked for not exceeding the geometric constraints. A total of 46 parameter set points are c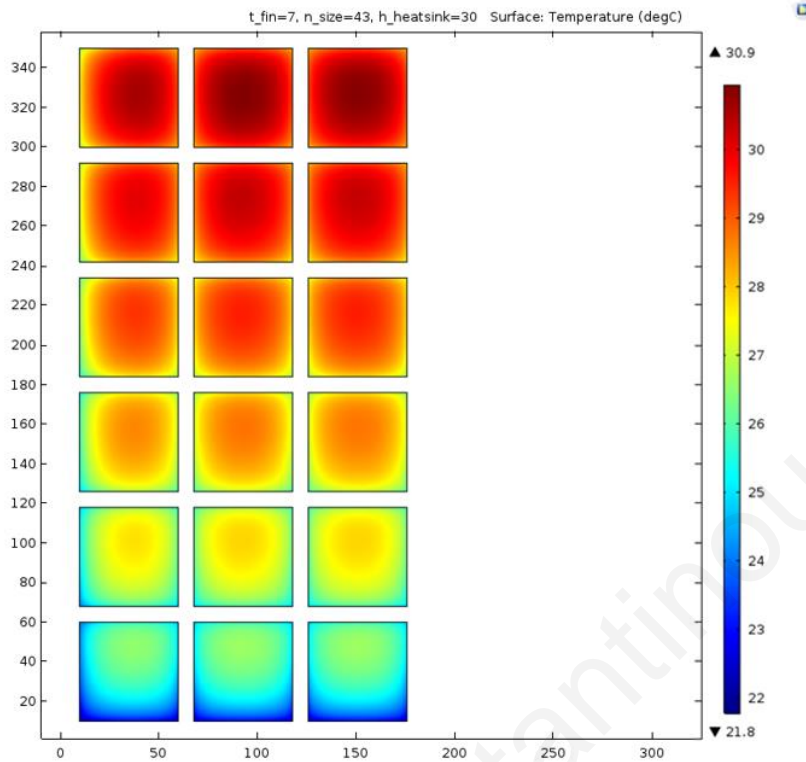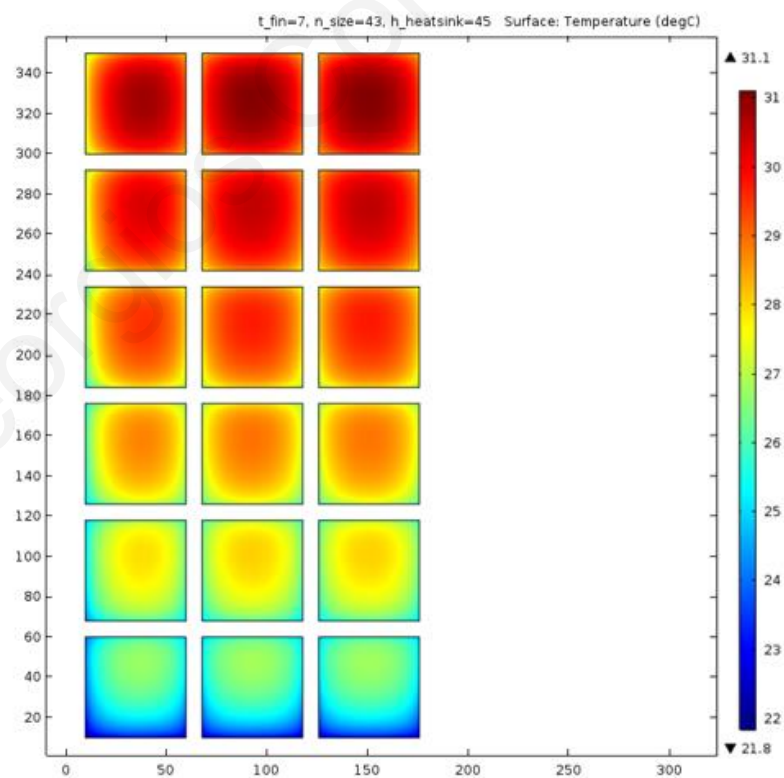reated and they are shown in the Appendix IV. The number of fins is constraint to be an odd integer number due to an unimportant model geometric limitation. These parameter set points are imported into COMSOL and simulated to produce the temperature distribution for each parameter set. The simulation results are then exported to MATLAB to calculate the produced power.

The results of the LHS parametric study are shown in Figure 5.6. The LHS parametric study provides a new maximum power of 368.3 W, which is produced by parameter set 10. The geometric parameters for producing this power are 6 mm fin thickness, 44 mm heatsink height, and 49 fins.
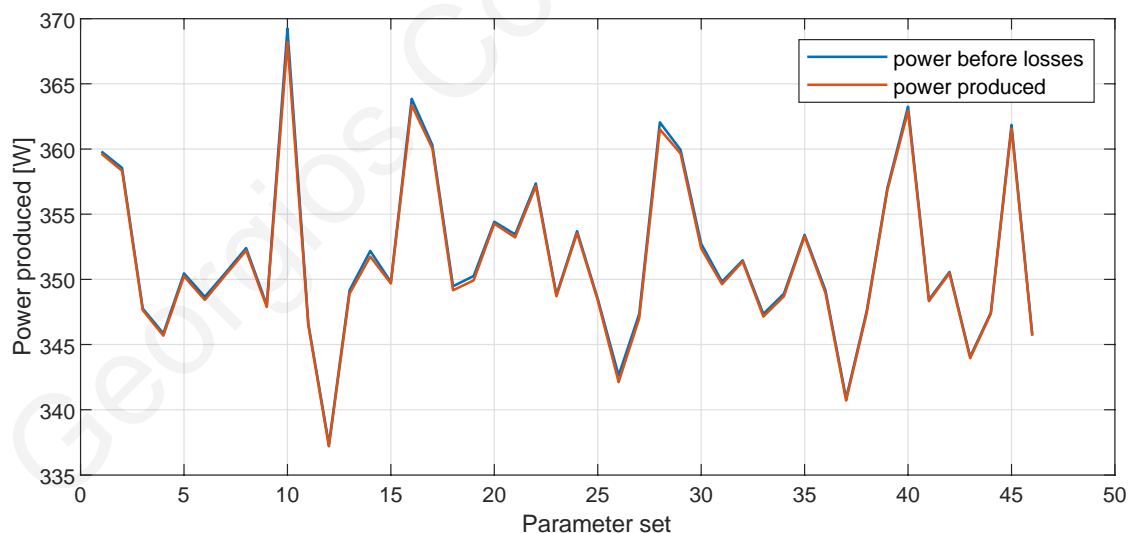
Figure 5.6: LHS parametric study results

Point 10 with the maximum net power provides also a new optimized set of parameters that the pressure difference and maximum temperature at cold plate are close to the results of point 25 and 26 from full factorial study. The pressure difference presented in Figure 5.7 is lower than the one at point 26 of full factorial. The maximum temperature in cold plate presented in Figure 5.8 is between the temperatures taken

from point 25 and 26. As expected, LHS was able to identify a better design as compared to the full factorial analysis.
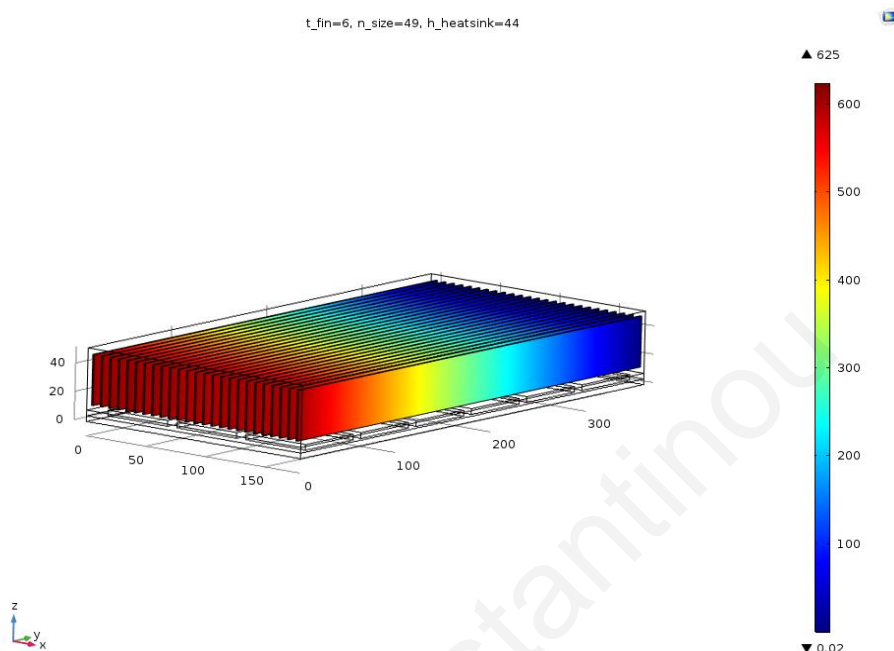
Figure 5.7:Pressure difference at point 10
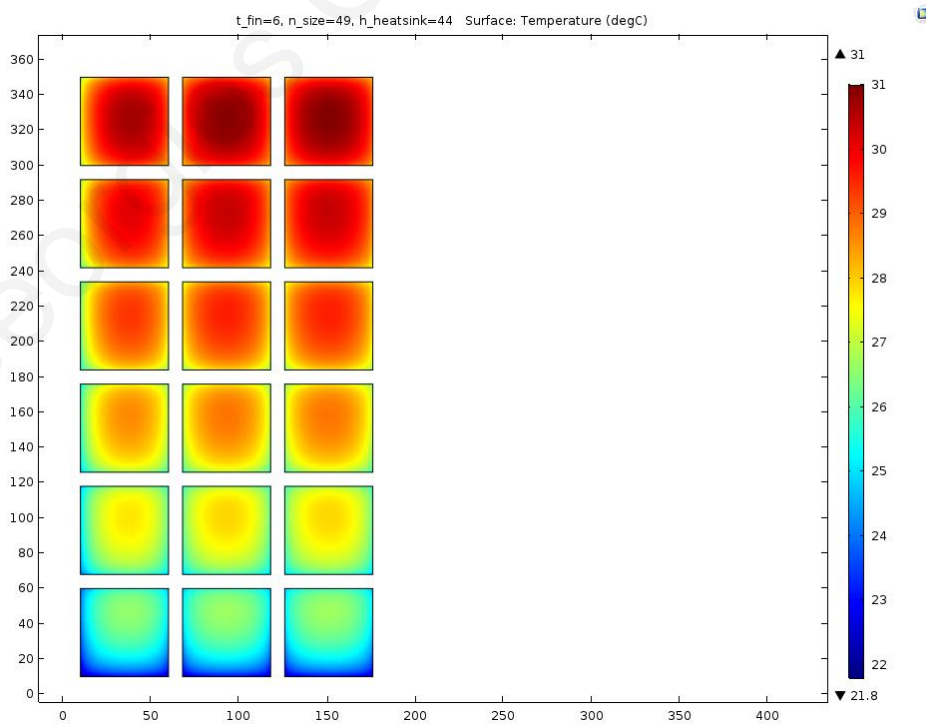
Figure 5.8:Temperature at cold plate for point 10

CHAPTER 6

6 CONCLUSIONS AND FUTURE WORK

Significant exhaust gases energy from maritime ICE engines can be recovered and converted into electricity with the use of a properly designed thermoelectric generator system. This "best" design is identified using a systematic design methodology and Latin Hypercube Sampling. More specifically an optimized heatsink for providing the lowest possible temperature at the cold side of the thermoelectric module is designed. This systematic methodology can be used for further optimization studies for this device or explore alternate installation positions on the ICE.

The design analyses are made possible by modeling and simulation that provides the required temperature distribution at the two sides of the thermoelectric modules. Proper and methodical building of the FEM model allows efficient simulation that in turn enables the investigation of multiple designs in short time.

The developed model will be used in future studies for further exploration of the design space by studying the effect of other device parameters to the produced power. In this study only the geometry of the heatsink and its effect to the performance of the device is considered. More simplifications can be studied such as exclude the heat expansion plate from the overall simulation. There are many other device parameters that affect the efficiency, and their contribution can be investigated using the proposed approach in this work. For example, different heatsink materials, patterns of thermoelectric modules, size of thermoelectric modules, cooling water flow rate, can be examined more efficiently using LHS, however this remains as future work.

References

1. Singh, D. V., and Pedersen, E., 2016, "A Review of Waste Heat Recovery Technologies for Maritime Applications," Energ Convers Manage, 111, pp. 315–328.

2. Kuroki, T., Kabeya, K., Makino, K., Kajihara, T., Kaibe, H., and Hachiuma, H., 2014. "Thermoelectric Generation Using Waste Heat in Steel Works." Journal of Electronic Materials 43(6), pp. 2405–2410.

3. Fotis Kyriakidis, Kim Sørensen, Shobhana Singh, Thomas Condra, "Modeling and optimization of integrated exhaust gas recirculation and multi-stage waste heat recovery in marine engines" ,Energy Conversion and Management, Volume 151, 2017, p. 286-295.

4. M.E. Mondejar, J.G. Andreasen, L. Pierobon, U. Larsen, M. Thern, F. Haglind, "A review of the use of organic Rankine cycle power systems for maritime applications" , Renewable and Sustainable Energy Reviews, Volume 91, 2018, p. 126-151

5. Ulrik Larsen, Tuong-Van Nguyen, Thomas Knudsen, Fredrik Haglind, "System analysis and optimisation of a Kalina split-cycle for waste heat recovery on large marine diesel engines", Energy, Volume 64, 2014, Pages 484-494, ISSN 0360-5442

6. X. Liu, C. Li, Y.D. Deng, C.Q. Su, An energy-harvesting system using thermoelectric power generation for automotive application,International Journal of Electrical Power & Energy Systems, Volume 67, 2015 ,Pages 510-516, ISSN 0142-0615, https://doi.org/10.1016/j.ijepes.2014.12.045.

7. Lee, J., Choo, S., Ju, H., Hong, J., Yang, S. E., Kim, F., Gu, D. H., Jang, J., Kim, G., Ahn, S., Lee, J. E., Kim, S. Y., Chae, H. G., Son, J. S., Doping-Induced Viscoelasticity in PbTe Thermoelectric Inks for 3D Printing of Power-Generating Tubes. *Adv.EnergyMater.* 2021, 11, 2100190. https://doi.org/10.1002/aenm.202100190

8. Song Lan, Richard Stobart, Xiaonan Wang,Matching and optimization for a thermoelectric generator applied in an extended-range electric vehicle for waste heat recovery,Applied Energy,Volume 313,2022,118783,ISSN 0306-2619,https://doi.org/10.1016/j.apenergy.2022.118783.

9. Kaibe, H., Makino, K., Kajihara, T., Fujimoto, S., and Hachiuma, H., 2012. "Thermoelectric generating system attached to a carburizing furnace at Komatsu Ltd., Awazu Plant." AIP Conference Proceedings 1449(1), 524-527.

10. Wei Yang, Heping Xie, Licheng Sun, Cheng Ju, Bixiong Li, Cunbao Li, Hongyin Zhang, Hongtao Liu, ''An experimental investigation on the performance of TEGs with a compact heat exchanger design towards low-grade thermal energy recovery'', Applied Thermal Engineering,Volume 194,2021, 117119.

11. Lee, J., Choo, S., Ju, H., Hong, J., Yang, S. E., Kim, F., Gu, D. H., Jang, J., Kim, G., Ahn, S., Lee, J. E., Kim, S. Y., Chae, H. G., and Son, J. S., 2021, "Doping-Induced Viscoelasticity in PbTe Thermoelectric Inks for 3D Printing of Power-Generating Tubes," Adv Energy Mater, 11(20), p. 2100190.

12. Snyder, X G. J. and Toberer, E. S., 2008. Complex thermoelectric materials. Nature materials, 2(7), pp. 105-114.

13. Pryor, R.W., 2011, "Multiphysics Modeling Using COMSOL: A First Principles Approach," Jones & Bartlett Learning, ISBN 978-0763779993.

14. COMSOL, Inc., 2017, "COMSOL Multiphysics Version 5.2 User's Guide."

15. Schenk, O., and Gärtner, K., 2004, "Solving Unsymmetric Sparse Systems of Linear Equations with PARDISO," Future Gener Comp Sy, 20(3), pp. 475–487.

16. Viana, F. A. C., 2016, "A Tutorial on Latin Hypercube Design of Experiments," Qual Reliab Eng Int, 32(5), pp. 1975–1985.

17. Stein, M., 1987, "Large Sample Properties of Simulations Using Latin Hypercube Sampling," Technometrics, 29(2), p. 143.

18. TECTEG MFR. https://thermoelectric-generator.com.

19. Bahrami, M., Yovanovich, M. M., & Culham, J. R. (2005). Pressure Drop of Fully-Developed, Laminar Flow in Microchannels of Arbitrary Cross-Section. https://doi.org/10.1115/icmm2005-75109

Appendix

Appendix I – 1D Model MATLAB script

```matlab
clear all
%table to array transformation
delimiterIn = ' ';
headerlinesIn = 0;
data2= importdata('data_profile.txt',delimiterIn,headerlinesIn);
dens=998;
x2=data2(:,1);
t2=data2(:,2);
%geometric constants
l=0.36;
d_cooper=0.004;
d_teg=0.004;
d_alum=0.004;
d_conv=0.052;
l_fin=0.04;
t=0.004;
a_teg=0.05*0.05;
%water parameters
viscw=1.1373*10^(-3);
cpw=4187;
Prw=9.46;
um=0.1;
%thermal conductivities
k_cooper=400;
k_alum=238;
k_teg=1.2;
k_air=0.026;
k_water=0.6;
Pr=(cpw*viscw)/k_water;


%calculations
lc=l_fin+t/2;

Re=(dens*um*d_conv)/viscw;
Nu=3.61+((0.065*(d_conv/l)*Re*Pr)/(1+0.016*(((d_conv/l)*Re*Pr)^(2/3)))
);
h=Nu*k_water/d_conv;
m=((2*h)/k_water*t)^(1/2);
eff=tanh(m*lc)/(m*lc);
eft=eff*1/100;
afin=2*l*lc;



 %total resistance calculations
R_fined=1/(h*afin*eft);
R_cooper=d_cooper/k_cooper;
R_teg=d_teg/(k_teg*a_teg);
R_alum=d_alum/k_alum;
R_tot=R_cooper+2*R_alum+R_fined+R_teg;
```

```matlab
DT=543-293;
Q=DT/R_tot;
%temperature values in specific positions
t(1)=543.15;
t(2)=t(1)-Q*R_cooper;
t(3)=t(2)-Q*R_teg;
t(4)=t(3)-Q*R_alum;
t(5)=t(4)-Q*R_fined;
t(6)=t(5)-Q*R_alum;
x=[0 0.004 0.008 0.012 0.064 0.068];
%data plot from comsol and matlab model
grid on
plot(x,t-275.15,'r')
hold on
plot(x2,t2-275.15)
grid on
ylabel('Temperature [°C]')
% xlabel('x(m)')
xticks([ 0 0.004 0.008 0.012 0.068])
xticklabels({'Manifold   ',  '     Plate', '    TEG', '
Heatsink start ', 'Heatsink end'})
legend('MATLAB model','COMSOL model')
sizefigure(6*96, 3*96, 50, 50, 50, 15, 10, [1 1],8, 9, 1)
```

Appendix II – Post processing MATLAB script

```matlab
%SYSTEM_INPUTS
%data_for_calculations
%LOADING DATA STEP
% Raw COMSOL 2D temp
% data_hot = load('data_hot.txt');
% data_cold = load('data_cold.txt');
data_hot = load('h27.txt');
data_cold = load('c27.txt');
%geometry inputs
t_fin=7;
n_size=45;
h_heatsink=60;
L=0.36;
Q_entry=0.0004;
dens=998.6;
visc=8.90*10^-4;
comsolp=22.4;
motorf=0.93;
pumpf=0.95;
module_area = 50*50;%mm^2
n =20; % Number of interpolation points (has to be odd)
% Module geometry pattern in x direction
x1 =10;
x2 =60;
x3 =68;
x4 =118;
x5 =126;
x6 =176;

% Module geometry pattern in y direction
y1=10;
y2=60;
y3=68;
y4=118;
y5=126;
y6=176;
y7=184;
y8=234;
y9=242;
y10=292;
y11=300;
y12=350;

% Module data
Tc_30=load('T=30.txt');
Tc_50=load('T=50.txt');
Tc_80=load('T=80.txt');
Tc_160(:,1) = Tc_80(:,1); % Add data for extrapolation
Tc_160(:,2) = Tc_80(:,2)*0.5;
Tc_15(:,1) = Tc_30(:,1);
Tc_15(:,2) = Tc_30(:,2)*1.15;

% Rearrange data
% Raw temp
x_h = data_hot(:,1);
y_h = data_hot(:,2);
T_h = data_hot(:,3);
x_c = data_cold(:,1);
y_c = data_cold(:,2);
T_c = data_cold(:,3);
```

```matlab
% Module data
mod_Tc(1:size(Tc_30,1),1)=30;
mod_Th(1:size(Tc_30,1),1)=Tc_30(:,1);
mod_P(1:size(Tc_30,1),1)=Tc_30(:,2);
mod_Tc(size(Tc_30,1)+1:size(Tc_30,1)+size(Tc_50,1),1)=50;
mod_Th(size(Tc_30,1)+1:size(Tc_30,1)+size(Tc_50,1),1)=Tc_50(:,1);
mod_P(size(Tc_30,1)+1:size(Tc_30,1)+size(Tc_50,1),1)=Tc_50(:,2);
mod_Tc(size(Tc_30,1)+size(Tc_50,1)+1:size(Tc_30,1)+size(Tc_50,1)+ …
size(Tc_80,1),1)=80;
mod_Th(size(Tc_30,1)+size(Tc_50,1)+1:size(Tc_30,1)+size(Tc_50,1)+ …
size(Tc_80,1),1)=Tc_80(:,1);
mod_P(size(Tc_30,1)+size(Tc_50,1)+1:size(Tc_30,1)+size(Tc_50,1)+ …
size(Tc_80,1),1)=Tc_80(:,2);
mod_Tc(size(Tc_30,1)+size(Tc_50,1)+size(Tc_80,1)+1:size(Tc_30,1)+ …
size(Tc_50,1)+size(Tc_80,1)+size(Tc_160,1),1)=160;
mod_Th(size(Tc_30,1)+size(Tc_50,1)+size(Tc_80,1)+1:size(Tc_30,1)+ …
size(Tc_50,1)+size(Tc_80,1)+size(Tc_160,1),1)=Tc_160(:,1);
mod_P(size(Tc_30,1)+size(Tc_50,1)+size(Tc_80,1)+1:size(Tc_30,1)+ …
size(Tc_50,1)+size(Tc_80,1)+size(Tc_160,1),1)=Tc_160(:,2);
mod_Tc(size(Tc_30,1)+size(Tc_50,1)+size(Tc_80,1)+size(Tc_160,1)+ …
1:size(Tc_30,1)+size(Tc_50,1)+size(Tc_80,1)+size(Tc_160,1)+ …
size(Tc_15,1),1)=15;
mod_Th(size(Tc_30,1)+size(Tc_50,1)+size(Tc_80,1)+size(Tc_160,1)+ …
1:size(Tc_30,1)+size(Tc_50,1)+size(Tc_80,1)+size(Tc_160,1)+ …
size(Tc_15,1),1)=Tc_15(:,1);
mod_P(size(Tc_30,1)+size(Tc_50,1)+size(Tc_80,1)+size(Tc_160,1)+ …
1:size(Tc_30,1)+size(Tc_50,1)+size(Tc_80,1)+size(Tc_160,1)+ …
size(Tc_15,1),1)=Tc_15(:,2);
clear data_in data_out Tc_30 Tc_50 Tc_80  Tc_160;


% Interpolate
% Interpolation ponts
x = [linspace(x1, x2, n) linspace(x3, x4, n) linspace(x5, x6, n)] ;
y = [linspace(y1, y2, n) linspace(y3, y4, n) linspace(y5, y6, n)
linspace(y7, y8, n) linspace(y9, y10, n) linspace(y11, y12, n) ]';
[xp, yp] = meshgrid(x,y);
% Hot surface
Th = griddata(x_h, y_h, T_h, xp, yp,'linear'); %'natural' , 'cubic'
Th_ave = mean(mean(Th));
% Cold surface
Tc = griddata(x_c, y_c, T_c, xp, yp,'linear'); %'natural' , 'cubic'
Tc_ave = mean(mean(Tc));


% Module power
cell_pow_F = scatteredInterpolant(mod_Tc(:), mod_Th(:), mod_P(:),
'linear', 'linear');
cell_pow = zeros(length(y)-1, length(x)-1);
cell_pow_plot = zeros(length(y)-1, length(x)-1);
for i=1:(length(y)-1)
    for j=1:(length(x)-1)
      cell_pow_plot(i,j) = NaN;
        if (i/n-floor(i/n))~=0 && (j/n-floor(j/n))~=0
            cell_area = (x(j+1) - x(j))*(y(i+1) - y(i));
            cell_Th = (Th(i,j) + Th(i,j+1) + Th(i+1,j) + Th(i+1,j))/4;
            cell_Tl = (Tc(i,j) + Tc(i,j+1) + Tc(i+1,j) + Tc(i+1,j))/4;
            cell_pow(i,j) = cell_pow_F(cell_Tl,
                cell_Th)*cell_area/module_area; %cell power
            cell_pow_plot(i,j) = cell_pow(i,j);
        end
    end
end
```

```matlab
end
Tcg=Tc;
Tcg(20,:) = NaN;
Tcg(40,:) = NaN;
Tcg(60,:) = NaN;
Tcg(80,:) = NaN;
Tcg(100,:) = NaN;
Tcg(:,20) = NaN;
Tcg(:,40) = NaN;
%STEP 1:Power as calculated from the modules
power = 2*sum(sum(cell_pow))


%STEP 2:Power needed to produce the water flow cooling condintions

%mathematical_expressions
lfin=h_heatsink-8;
Q_tube=Q_entry/(n_size+1);
L_Fin=(352-n_size*t_fin)/(n_size+1);
c=(L_Fin*10^-3)/2;
b=(lfin*10^-3)/2;
Entry_area=(L_Fin*(n_size+1)*lfin)*10^-6;
v_entry=Q_entry/Entry_area;
Dh=((2*lfin)/(lfin+L_Fin))*10^-3;
Re=(dens*v_entry*Dh)/visc;
%Pressure difference calculation
DP=(L*visc*v_entry)/((c^2)*((1/3)-
(64*c)/((3.14^5)*b)*tanh((3.14*b)/(2*c))));
f=64/Re;
hmaior=f*(L*v_entry^2)/(Dh*2);%
DP_friction=dens*hmaior;
DP_OVERALL=(DP+DP_friction);
Pwr_tube=Q_tube*DP_OVERALL/(motorf*pumpf);
Pwr_need=Pwr_tube*2*(n_size+1);
%INPUTS DP:Pressure difference Q:Volumetric flow
Overall_power=power-Pwr_need
%efficiency_calc
 max_p = cell_pow_F(20, 270)*36;
 efficiency=(Overall_power/max_p)*100;
% Plot Raw & Interpolated temperatures
figure(1)
plot3(x_h, y_h, T_h, 'r.')
hold on
surf(xp, yp, Th)
hold off

figure(2)
% plot3(x_c, y_c, T_c, 'b.');

view(-30,30)
hold on
mesh(x, y, Tcg-273.15)
hold off
grid on
xlabel('x [mm]','fontSize', 12);
ylabel('y [mm]','fontSize', 12)
zlabel('T [°C]','fontSize', 12)
set(gca,'DataAspectRatio',[1 1 0.1])
colorbar;
colorbar('eastoutside')
sizefigure(6*96, 5*96, 70, 10, 100, 5, 5, [1 1],8, 9, 1)
% Plot temperature difference
```

```matlab
figure(3)
mesh(x, y, Th-Tc)
set(gca,'DataAspectRatio',[1 1 0.1])
xlabel('x [mm]','fontSize', 12);
ylabel('y [mm]','fontSize', 12)
zlabel('\DeltaT [C]','fontSize', 12)


% Plot cell power
figure(4)
mesh(x(2:end), y(2:end), cell_pow_plot)
view(-30,30)
set(gca,'DataAspectRatio',[1 1 0.00002])
xlabel('x [mm]','fontSize', 12);
ylabel('y [mm]','fontSize', 12)
zlabel('P_{cell} [W]','fontSize', 12)
colorbar;
colorbar('eastoutside')
sizefigure(6*96, 5*96, 70, 10, 100, 5, 5, [1 1],8, 9, 1)
yl=mod_P(:,1);
zl=mod_Th(:,1);
xl=mod_Tc(:,1);
cl=[xl yl zl];
% figure(5)
% surf(cl)
```

Appendix III – Full factorial study

Study number	Fin thickness (t_fin)	Number of fins (n_size)	Heatsink height (h_hetsink)	Gross power	Net power	Power Losses
1	3	23	30	336.54	336.89	0.35
2	3	23	45	331.85	332.01	0.16
3	3	23	60	329.13	329.23	0.10
4	3	33	30	346.02	346.32	0.30
5	3	33	45	346.52	346.70	0.18
6	3	33	60	341.72	341.81	0.09
7	3	43	30	350.41	350.71	0.30
8	3	43	45	351.08	351.23	0.15
9	3	43	60	350.7	350.80	0.10
10	5	23	30	340.48	340.86	0.38
11	5	23	45	339.06	339.23	0.17
12	5	23	60	339.27	339.38	0.11
13	5	33	30	352.19	352.56	0.37
14	5	33	45	350.14	350.32	0.18
15	5	33	60	350.14	350.26	0.12
16	5	43	30	359.18	359.63	0.45
17	5	43	45	362.05	362.30	0.25
18	5	43	60	360.97	361.14	0.17
19	7	23	30	343.66	344.10	0.44
20	7	23	45	345.28	345.48	0.20
21	7	23	60	345.02	345.14	0.12
22	7	33	30	353.45	353.95	0.50
23	7	33	45	359.78	360.06	0.28
24	7	33	60	358.45	358.65	0.20
25	**7**	**43**	**30**	**367.35**	**369.23**	**1.88**
26	**7**	**43**	**45**	*367.83*	**368.92**	**1.09**
27	7	43	60	367	367.76	0.76

Appendix IV – LHS parameter study evaluation points

Param. Set #	Fin thickness [mm]	Number of fins	Heatsink height [mm]	Param. Set #	Fin thickness [mm]	Number of fins	Heatsink height [mm]
1	4	45	50	24	2	55	42
2	4	45	42	25	2	49	58
3	2	47	48	26	2	31	24
4	2	43	40	27	4	31	30
5	4	37	38	28	4	51	26
6	2	41	32	29	4	47	36
7	4	37	44	30	2	45	26
8	4	39	44	31	2	49	34
9	2	47	46	32	2	53	58
10	6	49	44	33	2	41	36
11	2	45	50	34	4	33	40
12	2	31	40	35	4	43	28
13	4	37	34	36	4	37	34
14	4	35	26	37	2	35	54
15	2	51	56	38	4	33	48
16	4	51	28	39	4	43	52
17	4	47	38	40	6	41	32
18	2	41	28	41	4	35	58
19	4	39	30	42	2	51	50
20	6	33	56	43	4	31	56
21	6	33	46	44	2	43	36
22	6	35	54	45	6	39	46
23	2	49	54	46	2	39	42